

# 7,8-Dihydroxyflavone is a direct inhibitor of pyridoxal phosphatase

## Reviewed Preprint

Revised by authors after peer review.

## About eLife's process

### Reviewed preprint version 2

May 2, 2024 (this version)

### Reviewed preprint version 1



January 4, 2024

### Posted to preprint server

October 5, 2023


### Sent for peer review

October 4, 2023

Marian Brenner, Christoph Zink, Linda Witzinger, Angelika Keller, Kerstin Hadamek, Sebastian Bothe, Martin Neuenschwander, Carmen Villmann, Jens Peter von Kries, Hermann Schindelin, Elisabeth Jeanclos , Antje Gohla 

Institute of Pharmacology and Toxicology, University of Würzburg, Germany • Rudolf Virchow Center for Integrative and Translational Bioimaging, University of Würzburg, Germany • Leibniz-Forschungsinstitut für Molekulare Pharmakologie-FMP, Berlin, Germany • Institute of Clinical Neurobiology, University Hospital, University of Würzburg, Germany

 [https://en.wikipedia.org/wiki/Open\\_access](https://en.wikipedia.org/wiki/Open_access)

 Copyright information

## Abstract

Vitamin B6 deficiency has been linked to cognitive impairment in human brain disorders for decades. Still, the molecular mechanisms linking vitamin B6 to these pathologies remain poorly understood, and whether vitamin B6 supplementation improves cognition is unclear as well. Pyridoxal phosphatase (PDXP), an enzyme that controls levels of pyridoxal 5'-phosphate (PLP), the co-enzymatically active form of vitamin B6, may represent an alternative therapeutic entry point into vitamin B6-associated pathologies. However, pharmacological PDXP inhibitors to test this concept are lacking. We now identify a PDXP and age-dependent decline of PLP levels in the murine hippocampus that provides a rationale for the development of PDXP inhibitors. Using a combination of small molecule screening, protein crystallography and biolayer interferometry, we discover, visualize and analyze 7,8-dihydroxyflavone (7,8-DHF) as a direct and potent PDXP inhibitor. 7,8-DHF binds and reversibly inhibits PDXP with low micromolar affinity and sub-micromolar potency. In mouse hippocampal neurons, 7,8-DHF increases PLP in a PDXP-dependent manner. These findings validate PDXP as a druggable target. Of note, 7,8-DHF is a well-studied molecule in brain disorder models, although its mechanism of action is actively debated. Our discovery of 7,8-DHF as a PDXP inhibitor offers novel mechanistic insights into the controversy surrounding 7,8-DHF-mediated effects in the brain.

### eLife assessment

Following small molecule screens, this study provides **convincing** evidence that 7,8-dihydroxyflavone (DHF) is a competitive inhibitor of pyridoxal phosphatase. These results are **important** since they offer an alternative mechanism for the effects of 7,8-dihydroxyflavone in cognitive improvement in several mouse models. This paper is also significant due to the interest in the phosphatases and neurodegeneration fields.

## Introduction

Vitamin B6 is an essential micronutrient that plays an important role in the nervous system (1, 2), with the vitamin B6 status affecting cognitive function at any age (3, 4). Population studies indicate that low vitamin B6 levels are common among older people (5), and suggest that vitamin B6 deficiency may influence memory performance and may contribute to age-related cognitive decline (6–9). Vitamin B6 deficiency is also associated with other conditions characterized by impaired learning and memory, including neuropsychiatric disorders (10–12), Alzheimer's disease (13) and inflammation (14, 15). Nevertheless, the exact molecular mechanisms linking vitamin B6 to these pathologies are often insufficiently understood, and whether vitamin B6 supplementation improves cognition is unclear (4, 5, 16–22).

The term vitamin B6 encompasses the enzymatically interconvertible compounds pyridoxine, pyridoxamine, pyridoxal (collectively referred to as B6 vitamers) and their phosphorylated forms. Among these, only pyridoxal 5'-phosphate (PLP) is co-enzymatically active. In humans, PLP is known to be required for 44 distinct biochemical reactions, including the biosynthesis and/or metabolism of neurotransmitters, amino acids, lipids, and glucose. In addition, B6 vitamers display antioxidant and anti-inflammatory functions (23–26).

Cellular PLP availability in the brain depends on numerous factors, including the intestinal absorption of B6 vitamers, extracellular phosphatases, inter-organ transport and intracellular enzymes and carriers/scavengers involved in PLP formation and homeostasis (2). Specifically, intracellular PLP is formed by the pyridoxal kinase (PDXK)-catalyzed phosphorylation of pyridoxal, or the pyridox(am)ine-5'-phosphate oxidase (PNPO)-catalyzed oxidation of pyridox(am)ine 5'-phosphate to PLP. PLP is highly reactive and can undergo condensation reactions with e.g., primary amino groups or thiol groups in proteins or amino acids. Although the mechanisms of PLP delivery within the cells are still largely unknown, it is clear that the intracellular availability of PLP for co-enzymatic functions depends on PLP carriers/scavengers and on the hydrolytic activity of pyridoxal 5'-phosphate phosphatase (PDXP) (2, 27–30).

We have previously shown that the genetic knockout of PDXP (PDXP-KO) in mice increases brain PLP levels and improves spatial memory and learning, suggesting that elevated PLP levels can improve cognitive functions in this model (30). We therefore reasoned that a pharmacological inhibition of PDXP may be leveraged to increase intracellular PLP levels and conducted a high-throughput screening campaign to identify small-molecule PDXP modulators. Here, we report the discovery and the structural and cellular validation of 7,8-dihydroxyflavone (7,8-DHF) as a preferential PDXP inhibitor. 7,8-DHF is a well-studied molecule in brain disorder models characterized by impaired cognition, and widely regarded as a tropomyosin receptor kinase B (TrkB) agonist with brain-derived neurotrophic factor (BDNF)-mimetic activity (31). However, a direct TrkB agonistic activity of 7,8-DHF has been called into question (32–36). Our serendipitous discovery of 7,8-DHF as a direct PDXP inhibitor provides an alternative mechanistic explanation for 7,8-DHF-mediated effects. More potent, efficacious, and selective PDXP inhibitors may be useful future tools to explore a possible benefit of elevated PLP levels in brain disorders.

## Results

### PDXP activity controls PLP levels in the hippocampus

The hippocampus is important for age-dependent memory consolidation and learning, and impaired memory and learning is associated with PLP deficiency (3). To study a possible contribution of PDXP and/or PDXK to age-related PLP homeostasis in the hippocampus, we performed Western blot analyses in young versus older mice. Unexpectedly, we found that both PDXP and PDXK expression levels were markedly higher in hippocampi of middle-aged than of juvenile animals (Fig. 1a). These data suggest an accelerated hippocampal PLP turnover in older mice, consistent with previous findings in senescent mice (37).

An analysis of total hippocampal PLP levels in PDXP-WT and PDXP-KO mice showed an age-dependent profile. PLP levels appeared to peak around 3 months of age (possibly reflecting PLP-dependent neurotransmitter biosynthesis and metabolism during the postnatal developmental period) and descended back to juvenile levels by 12 months of age in both genotypes. Although total hippocampal PLP levels in PDXP-KO mice also decreased with age, they consistently remained above PLP levels in control mice (Fig. 1b; two-tailed, unpaired *t*-test of PLP levels in PDXP-WT vs. PDXP-KO hippocampi, all ages combined:  $p < 0.0001$ ).

PLP is protected from hydrolysis by binding to proteins, and PDXP is expected to dephosphorylate only non-protein-bound PLP (38). To test this, we prepared protein-depleted PLP fractions from PDXP-WT and PDXP-KO hippocampal lysates using 3 kDa molecular weight cutoff centrifugal filters. The quantification of PLP in these fractions demonstrated that PDXP loss indeed only increased the pool of protein-depleted PLP, both in young (18–42 days old) and older mice (252–352 days old, corresponding to mature/middle-aged mice), whereas the levels of protein-bound PLP remained unchanged (Fig. 1c). While the hippocampal levels of non-protein-bound PLP dropped by about 60% over this time span in PDXP-WT mice, they remained elevated in PDXP-KO mice (~2-fold higher in younger, and ~5-fold higher in older PDXP-KO compared to the respective PDXP-WT; see Fig. 1 – figure supplement 1 for exact mouse ages). We conclude that hippocampi of older mice are characterized by a specific decrease in the levels of non-protein-bound PLP, and that this age-dependent PLP loss is dependent on PDXP activity. These observations establish that PDXP is a critical determinant of PLP levels in the murine hippocampus and suggest that intracellular PLP deficiency may be alleviated by PDXP inhibition.

### A high-throughput screening campaign identifies 7,8-dihydroxyflavone as a PDXP inhibitor

Pharmacological small-molecule PDXP inhibitors are currently lacking. To identify PDXP inhibitor candidates, we screened the FMP small molecule repository containing 41,182 compounds for molecules able to modulate the phosphatase activity of recombinant, highly purified murine PDXP (see Fig. 2 – figure supplement 1 for a schematic of the screening campaign). Difluoro-4-methylumbelliferyl phosphate (DiFMUP) was used as a fluorogenic phosphatase substrate in a primary screen. Compounds that altered DiFMUP fluorescence by  $\geq 50\%$  (activator candidates) or  $\leq 25\%$  (inhibitor candidates) were subjected to  $EC_{50}/IC_{50}$  value determinations. Of these, 46 inhibitor hits were selected and counter-screened against phosphoglycolate phosphatase (PGP), the closest PDXP relative (39, 40). Eleven of the PDXP inhibitor hits (with an  $IC_{50}$  PDXP  $< 20$   $\mu$ M, and  $IC_{50}$  PDXP  $< IC_{50}$  PGP or no activity against PGP) were subsequently validated in a secondary assay, using PLP as a physiological PDXP substrate (see Fig. 2 – figure supplement 2 for all 11 inhibitor hits). Only one PDXP-selective inhibitor hit (7,8-dihydroxyflavone/7,8-DHF, a naturally occurring flavone) blocked PDXP-catalyzed PLP dephosphorylation ( $IC_{50} \sim 1$   $\mu$ M).

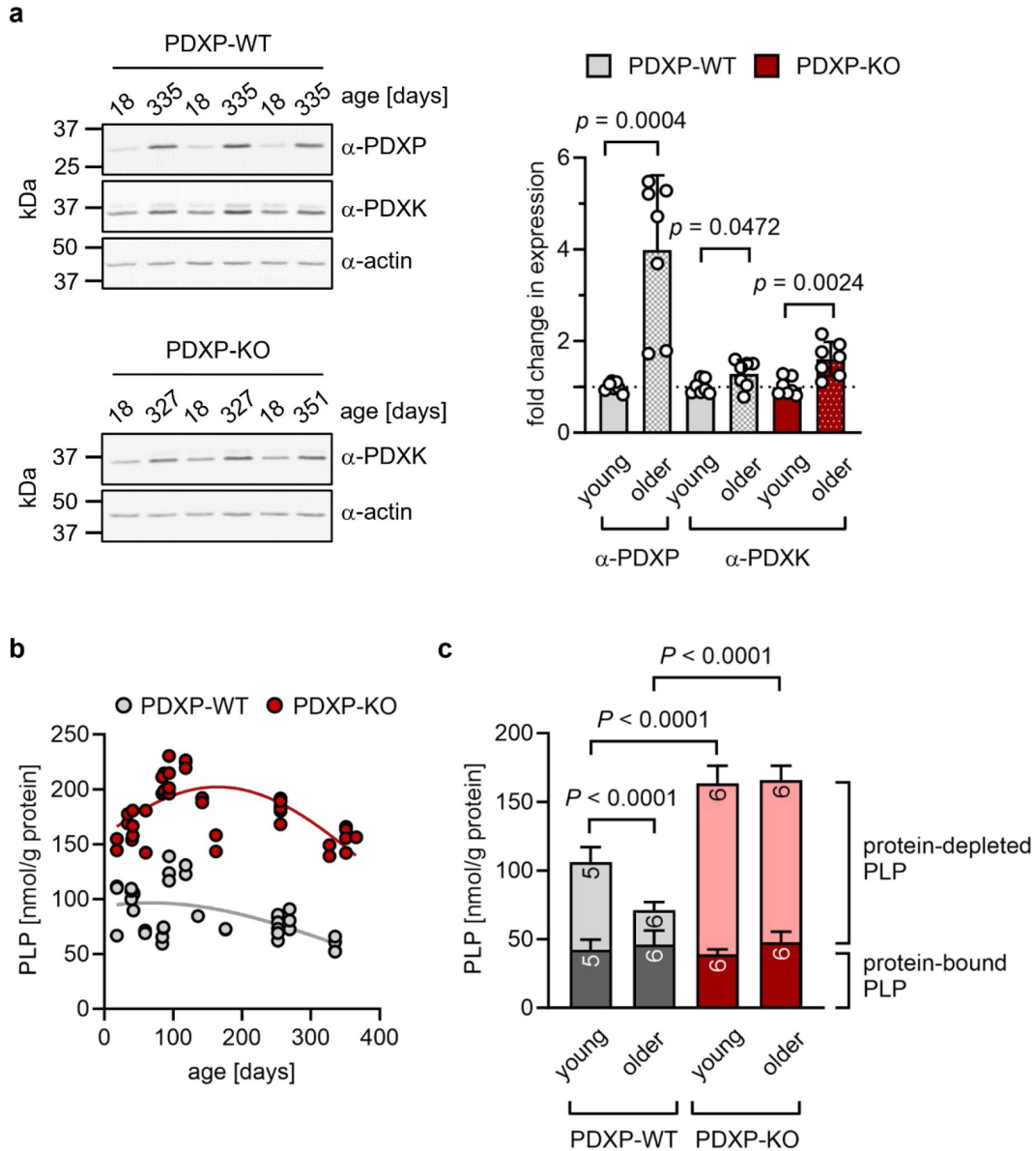


**Figure 1.**

**Role of PDXP in hippocampal PLP homeostasis.**

(a) Age-dependent expression of PDXK and PDXP in murine hippocampi. *Left panels*, representative Western blots of three hippocampi for each genotype. The same blots were reprobbed with  $\alpha$ -actin antibodies as a loading control. The age of the investigated mice is indicated above the blots. *Right panel*, densitometric quantification of hippocampal PDXP and PDXK Western blot signals, corrected by the corresponding actin signals. Young mice were 18-42 days old, older mice were 252-351 days old;  $n=7$  hippocampi were analyzed per group. Data are mean values  $\pm$  S.D. Statistical analysis was performed with unpaired, two-sided *t*-tests; *p*-values are indicated. (b) Age-dependent, total PLP-concentrations in isolated hippocampi of PDXP-WT and PDXP-KO mice. PLP was derivatized with semicarbazide and analyzed by HPLC. Each symbol represents the result of the PLP determination in an individual hippocampus. Data were fitted by Gaussian least-squares analyses. (c) Determination of protein-bound and protein-depleted PLP in PDXP-WT and PDXP-KO hippocampal lysates of young (18-42 days old) and older mice (252-352 days old). The number of analyzed hippocampi is indicated in the bars. Data are mean values  $\pm$  S.D. Statistical analysis was performed with two-way ANOVA and Tukey's multiple comparisons test. Significant differences (adjusted *P*-values) in protein-depleted PLP levels are indicated. The exact age of analyzed mice is listed in **Figure 1 - supplementary figure 1** [↗](#). **Source data** are available for this Figure.

In vitro activity assays using PLP as a substrate confirmed that 7,8-DHF directly blocks murine and human PDXP activity with submicromolar potency and an apparent efficacy of ~50% (**Fig. 2a**, **b**). We next examined whether commercially available 7,8-DHF analogs might be more potent or efficacious PDXP inhibitors. We tested flavone, 3,7-dihydroxyflavone, 5,7-dihydroxyflavone (also known as chrysin), 3,5,7-trihydroxyflavon (galangin), 5,6,7-trihydroxyflavone (baicalein) and 3,7,8,4'-tetrahydroxyflavone. **Figure 2b** shows that of the tested 7,8-DHF analogs, only 3,7,8,4'-tetrahydroxyflavone was able to inhibit PDXP, albeit with an  $IC_{50}$  of 2.5  $\mu\text{M}$  and thus slightly less potently than 7,8-DHF. These results suggest that hydroxyl groups in positions 7 and 8 of the flavone scaffold are required for PDXP inhibition. The efficacy of PDXP inhibition by 3,7,8,4'-tetrahydroxyflavone was not substantially increased at concentrations  $>40 \mu\text{M}$  (relative PDXP activity at 40  $\mu\text{M}$ :  $0.46 \pm 0.05$ ; at 70  $\mu\text{M}$ :  $0.38 \pm 0.15$ ; at 100  $\mu\text{M}$ :  $0.37 \pm 0.09$ ; data are mean values  $\pm$  S.D. of  $n=6$  experiments). Concentrations  $>100 \mu\text{M}$  could not be assessed due to impaired PDXP activity at the DMSO concentrations required for solubilizing the flavone.

We used a biolayer interferometry (BLI) optical biosensing technique to further characterize the binding of 7,8-DHF to PDXP (**Fig. 2c**). Consistent with a specific interaction, 7,8-DHF binding to PDXP was concentration-dependent and fully reversible. As a result of the poor solubility of the molecule, a saturation of the binding site was not experimentally accessible. Steady-state analysis of a 7,8-DHF serial dilution series yielded an affinity ( $K_D$ ) value of  $3.1 \pm 0.3 \mu\text{M}$  (data are mean values  $\pm$  S.E. of  $n=4$  measurements; see **Fig. 2 – figure supplement 3** for the three other measurements) using a 1:1 dose-response model. Global analysis of the sensorgrams assuming a 1:1 binding model resulted in an affinity of  $2.6 \pm 0.5 \mu\text{M}$ , in line with the steady-state results (**Fig. 2c**). As expected, 5,7-dihydroxyflavone showed no signal in the BLI, in line with previous experiments (see **Fig. 2b**). With its molecular size of 254 Da and its physicochemical properties, 7,8-DHF is a typical fragment-like molecule (41). Typical association rate constants ( $k_{\text{on}}$ ) for fragments are limited by the rate of diffusion and are higher than  $10^6 \cdot \text{M}^{-1} \text{s}^{-1}$ . Interestingly, 7,8-DHF showed a slow  $k_{\text{on}}$  of  $1.05 \cdot 10^4 \text{ M}^{-1} \text{s}^{-1}$ , which is atypical and rarely found for fragment-like molecules (42), and a  $k_{\text{off}}$  rate of  $0.03 \text{ s}^{-1}$ . With the commonly used estimation of  $\Delta G \sim pK_D$  and a heavy atom number of 19, 7,8-DHF shows a high ligand efficiency of 0.39, which makes it an interesting molecule for further medicinal chemistry optimization. Taken together, these data support a direct and reversible physical interaction between 7,8-DHF and PDXP that leads to PDXP inhibition.

## Selectivity of 7,8-DHF

PDXP is a member of the large family of haloacid dehalogenase (HAD)-type hydrolases (43). HAD phosphatases are  $\text{Mg}^{2+}$ -dependent phospho-aspartate transferases that consist of a Rossmann-like catalytic core linked to a cap domain. The insertion site, structure and size of the cap define the substrate selectivity of the respective enzyme. The “capless” C0-type HAD phosphatases contain either a very small or no cap, resulting in an accessible catalytic cleft that enables the dephosphorylation of macromolecular substrates. Larger C1 or C2 caps act as a roof for the entrance to the active site; most C1/C2-capped HAD phosphatases consequently dephosphorylate small molecules that can gain access to the catalytic cleft. Cap domains also contain so-called substrate specificity loops that contribute to substrate coordination. Hence, caps are distinguishing features of HAD phosphatases (38, 43–45).

To probe the selectivity of 7,8-DHF for PDXP, a C2-capped HAD phosphatase, we tested eight other mammalian HAD phosphatases, including two other C2-, four C1- and two C0-type enzymes. In addition, we analyzed the activity of 7,8-DHF towards the prototypical tyrosine phosphatase PTP1B (which is known to be sensitive to specific flavonoids, ref. (46)); the serine/threonine protein phosphatase calcineurin (PP2B); and a DNA/RNA-directed alkaline phosphatase (calf intestinal phosphatase, CIP) (**Fig. 2d**). When assayed at nominal concentrations of 5, 10 and 40  $\mu\text{M}$  (i.e., up to ~40-fold above the  $IC_{50}$  value for PDXP-catalyzed PLP-dephosphorylation), 7,8-DHF was completely inactive against six of the tested enzymes. At the highest tested concentration of 40  $\mu\text{M}$ , 7,8-DHF weakly inhibited PTP1B and the polynucleotide kinase-3'-phosphatase PNKP and

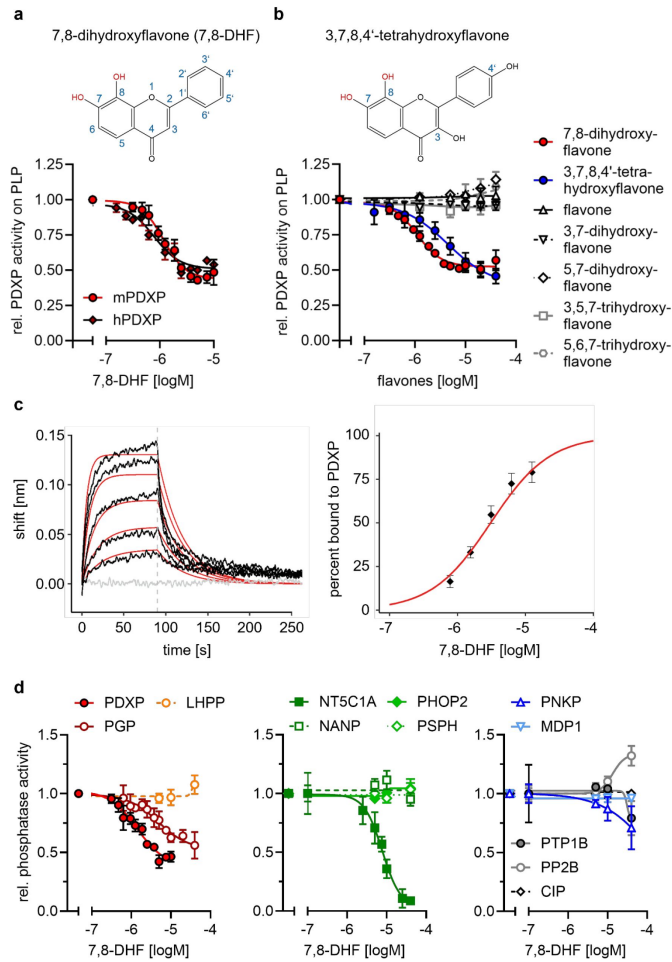


**Figure 2**

### Characterization of the 7,8-DHF/PDXP interaction.

(a) Determination of half-maximal inhibitory constants ( $IC_{50}$ ) of 7,8-DHF (2D-structure shown on top) for purified murine or human PDXP, using pyridoxal 5'-phosphate (PLP) as a substrate. Phosphatase activities in the presence of 7,8-DHF were normalized to the respective enzyme activities measured in the presence of the DMSO solvent control. Data are mean values  $\pm$  S.D. of  $n=3$  (human PDXP) and  $n=4$  (murine PDXP) independent experiments. (b)  $IC_{50}$  values of different flavones for purified murine PDXP with PLP as a substrate. Phosphatase activities in the presence of flavones were normalized to the respective enzyme activities in the presence of the DMSO solvent control. All data are mean values  $\pm$  S.D. The inhibition of PDXP by 3,7,8-trihydroxyflavone-4'-hydroxyphenyl (2D-structure shown on top) was assessed in  $n=6$  independent experiments. All other data are from  $n=3$  biologically independent experiments. Apparently missing error bars are hidden by the symbols. (c) Biolayer interferometry (BLI) measurements of the interaction of 7,8-DHF with purified murine PDXP. *Left panel*, example sensorgram overlaid with the global 1:1 binding model (red) and the negative control (gray). The dashed line indicates the start of the dissociation phase. *Right panel*, steady-state dose-response analysis for 7,8-DHF based on  $n=4$  measurements. (d) Sensitivity of the indicated phosphatases to 7,8-DHF. Phosphatase activities in the presence of 7,8-DHF were normalized to the respective enzyme activities measured in the presence of the DMSO solvent control. Data are mean values  $\pm$  S.D. of  $n=4$  (PGP) or  $n=3$  independent experiments (all other phosphatases). Phosphatase substrates and HAD phosphatase cap types are indicated in parentheses. PDXP, pyridoxal-5'-phosphate phosphatase (pyridoxal 5'-phosphate; C2); PGP, phosphoglycolate phosphatase (2-phosphoglycolate; C2); LHPP, phospholysine phosphohistidine inorganic pyrophosphate phosphatase (imidodiphosphate; C2); NT5C1A, soluble cytosolic 5'-nucleotidase 1A (AMP; C1); NANP, N-acetylneuraminatate 9-phosphate phosphatase (6-phosphogluconate; C1); PHOP2, phosphatase orphan 2 (pyridoxal 5'-phosphate; C1); PSPH, phosphoserine phosphatase (O-phospho-L-serine; C1); PNKP, polynucleotide kinase phosphatase (3-phospho-oligonucleotide; C0); MDP1, magnesium-dependent phosphatase-1 (D-ribose-5-phosphate; C0); PTP1B (protein tyrosine phosphatase 1B; EGFR phospho-peptide); PP2B, protein phosphatase 2B/calcineurin (PKA regulatory subunit type II phospho-peptide); CIP, calf intestinal phosphatase ( $\rho$ NPP). **Source data** are available for this Figure.

appeared to increase the activity of calcineurin. As expected, 7,8-DHF inhibited PGP, the closest PDXP relative, with an  $IC_{50}$  value of 4.8  $\mu M$ . This result is consistent with the criteria applied during the initial counter-screen (see above). In addition to PGP, 7,8-DHF inhibited the C1-capped soluble cytosolic 5'-nucleotidase 1A (NT5C1A) with an  $IC_{50}$  value of  $\sim 10$   $\mu M$ . NT5C1A is an AMP hydrolase expressed in skeletal muscle and heart (47 [↗](#)), which is also sensitive to inhibition by small molecules that target the closest PDXP-relative PGP (40 [↗](#)). Together, the selectivity analysis of 7,8-DHF on a total of 12 structurally and functionally diverse protein- and non-protein-directed phosphatases show that 7,8-DHF preferentially inhibits PDXP, and that higher 7,8-DHF concentrations can also target the PDXP paralog PGP and the nucleotidase NT5C1A.

## Mode of PDXP inhibition

To probe the mechanism of PDXP inhibition, we assayed the steady state kinetics of PLP dephosphorylation in the presence of increasing 7,8-DHF concentrations (Table 1 [↗](#)). Analysis of the derived kinetic constants demonstrated that 7,8-DHF increased the  $K_M$  up to  $\sim 2$ -fold, and slightly reduced  $v_{max}$  values  $\sim 0.7$ -fold. Thus, 7,8-DHF mainly exhibits a mixed mode of PDXP inhibition, which is predominantly competitive.

## Co-crystal structures of PDXP bound to 7,8-DHF

To investigate the mechanism of PDXP inhibition in more detail, we co-crystallized homo-dimeric, full-length murine and human PDXP (mPDXP, hPDXP) with this compound. 7,8-DHF-bound murine PDXP co-crystallized with phosphate in the cubic space group I23, with protomer A containing the inhibitor and protomer B representing an inhibitor-free state (Fig. 3 – figure supplement 1a [↗](#)). The structure was refined following molecular replacement with full-length murine PDXP (here referred to as apo-mPDXP; Protein Data Bank/PDB entry 4BX3) to a resolution of 2.0  $\text{\AA}$  resulting in an  $R_{work}$  of 18.4% and an  $R_{free}$  of 21.1% (PDB code 8QFW). We additionally obtained two co-crystal structures of human PDXP with 7,8-DHF; one in a phosphate-containing, and one in a phosphate-free form. Both forms crystallized in the tetragonal space group P 4<sub>3</sub>2<sub>1</sub>2, and each protomer of both structures contained the inhibitor (Fig. 3a [↗](#)). These structures were refined following molecular replacement with full-length human PDXP (PDB entry 2P27, here referred to as apo-hPDXP) to a resolution of 1.5  $\text{\AA}$  resulting in an  $R_{work}/R_{free}$  of 17.0/19.4% (phosphate-bound 7,8-DHF-hPDXP, PDB code 9EM1), and to a resolution of 1.5  $\text{\AA}$  resulting in an  $R_{work}/R_{free}$  of 18.2/20.5% (phosphate-free 7,8-DHF-hPDXP, PDB code 8S8A). Data collection and refinement statistics are summarized in Table 2 [↗](#).

Like their respective apo-forms, 7,8-DHF-bound murine and human PDXP homodimerize via their cap domains (Fig. 3a [↗](#) and Fig. 3 – figure supplement 1a [↗](#)). The C $\alpha$  atom-based alignment of the structures representing murine apo-PDXP and murine 7,8-DHF-bound PDXP resulted in root mean square (RMS) deviations in the range of 0.43-0.71  $\text{\AA}$ . Even smaller values were obtained when human apo-PDXP, human PLP-bound PDXP and human 7,8-DHF-bound PDXP were superimposed with RMS deviations in the range from 0.29-0.54  $\text{\AA}$  (Table 3 [↗](#)). Hence, binding of the inhibitor did not result in significant changes in murine or human PDXP backbone conformations. All catalytic core residues and the Mg<sup>2+</sup> cofactor are correctly oriented in the presence of the inhibitor. We conclude that 7,8-DHF binding does not appear to impact the overall fold of murine or human PDXP.

7,8-DHF was observed to only bind to one subunit (the A-chain) of murine PDXP (Fig. 3 – figure supplement 1a [↗](#)) with well-defined density (Fig. 3 – figure supplement 1b [↗](#)) and full occupancy since its average B-factor of 45.8  $\text{\AA}^2$  closely matches the B-factors of the surrounding atoms. Binding to the other subunit (B-protomer) is prevented by a salt bridge between Arg62 and Asp14 of a symmetry-related A-protomer in the crystal (Fig. 3 – figure supplement 1c [↗](#)). The  $\chi_1$  and  $\chi_2$  torsion angles of the Arg62 side chain observed in the B-protomer correspond to those observed for this side chain in both protomers of the murine apo-structure (4BX3). To allow

7,8-DHF [ $\mu\text{M}$ ]	0	1.0	1.5	2.0	3.0	5.0	10.0
$K_M$ [ $\mu\text{M}$ ]	14.98 $\pm 1.28$	18.54 $\pm 6.24$	20.20 $\pm 6.19$	18.97 $\pm 5.15$	24.83 $\pm 2.61$	32.96 $\pm 2.13$	30.61 $\pm 2.57$
$v_{\text{max}}$ [ $\mu\text{mol}/\text{min}/\text{mg}$ ]	1.08 $\pm 0.04$	0.95 $\pm 0.01$	0.89 $\pm 0.04$	0.85 $\pm 0.02$	0.80 $\pm 0.04$	0.81 $\pm 0.05$	0.74 $\pm 0.06$
$k_{\text{cat}}$ [ $\text{s}^{-1}$ ]	0.57 $\pm 0.02$	0.5 $\pm 0.01$	0.47 $\pm 0.02$	0.45 $\pm 0.01$	0.42 $\pm 0.02$	0.43 $\pm 0.03$	0.39 $\pm 0.03$
$k_{\text{cat}}/K_M$ [ $\text{s}^{-1}\cdot\text{M}^{-1}$ ] ( $\times 10^{-4}$ )	3.93 $\pm 0.29$	3.27 $\pm 0.84$	2.75 $\pm 0.67$	2.72 $\pm 0.66$	1.72 $\pm 0.10$	1.31 $\pm 0.06$	1.29 $\pm 0.01$

The data are mean values  $\pm$  S.E.M. of  $n=3$  independent experiments, except for the solvent control samples ( $n=6$ ). Curves were fitted and parameters  $K_M$  (Michaelis–Menten constant);  $v_{\text{max}}$ , (maximum enzyme velocity);  $k_{\text{cat}}$  (turnover number) were derived using the Michaelis–Menten model in GraphPad Prism 9.5.1. The  $k_{\text{cat}}$  values were calculated from the maximum enzyme velocities using a molecular mass of 31,828 Da for PDXP. DMSO concentrations were kept constant (0.1% DMSO under all conditions, including the solvent control samples). **Source data** are available for this Table.

**Table 1.**

**Kinetic constants of PDXP-catalyzed PLP hydrolysis in the presence of 7,8-DHF.**



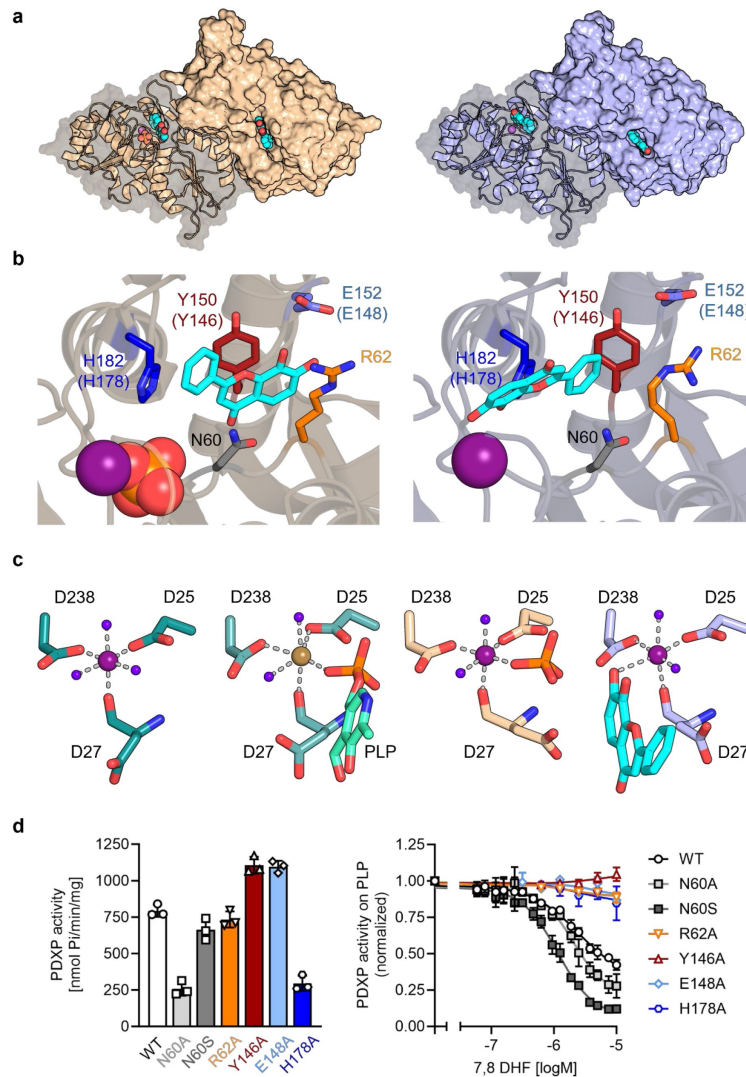


**Figure 3.**

### X-ray crystal structures of human PDXP in complex with 7,8-DHF.

(a) The models were refined to a resolution of 1.5 Å for full-length human 7,8-DHF-PDXP with phosphate (PDB code 9EM1, colored in wheat yellow, *left panel*) and 1.5 Å for full-length human 7,8-DHF-PDXP without phosphate (PDB code 8S8A, colored in light blue, *right panel*). One protomer of each homodimeric PDXP is shown in cartoon representation and the other protomer in surface representation. 7,8-DHF is displayed in sphere representation with its C-atoms in cyan. Mg<sup>2+</sup> ions are shown as deep purple spheres and phosphate ions are shown in sphere representation with the phosphorous atom in orange. (b) Orientation of 7,8-DHF in the active sites of human 7,8-DHF-PDXP in the presence or absence of phosphate. Structural details of bound 7,8-DHF and adjacent residues of the active sites are shown. *Left*, phosphate-containing 7,8-DHF-PDXP (wheat yellow, cartoon representation). *Right*, phosphate-free 7,8-DHF-PDXP (light blue, cartoon representation). 7,8-DHF is shown in stick representation (cyan C-atoms). The corresponding amino acids in murine PDXP are given in parentheses (see also **Fig. 3 – figure supplement 1e, f**). (c) Comparison of the Mg<sup>2+</sup> coordination spheres. *From left to right*: human apo-PDXP (PDB: 2P27), human PDXP in complex with PLP (PDB: 2CFT), human PDXP in complex with 7,8-DHF in the presence of phosphate (PDB: 9EM1), human PDXP in complex with 7,8-DHF in the absence of phosphate (PDB: 8A8S). The catalytically essential Mg<sup>2+</sup> is shown as a deep purple sphere. In 2CFT, Mg<sup>2+</sup> was exchanged for Ca<sup>2+</sup>, which is shown here as a light brown-colored sphere. Water molecules are shown as blue spheres. (d) Verification of 7,8-DHF - PDXP interactions. *Left panel*, phosphatase activity of purified PDXP or the indicated PDXP variants. Data are mean values ± S.D. of *n*=3 independent experiments. *Right panel*, determination of the IC<sub>50</sub> values of 7,8-DHF for purified PDXP or the indicated PDXP variants. Data are mean values ± S.D. of *n*=3 independent experiments. Apparently missing error bars are hidden by the symbols. **Source data** are available for this Figure.

	mPDXP-7,8-DHF with Phosphate (8QFW)	hPDXP-7,8-DHF with Phosphate (9EM1)	hPDXP-7,8-DHF without Phosphate (8S8A)
<b>Data collection</b>			
Space group	I23	P4 <sub>3</sub> 2 <sub>1</sub> 2	P4 <sub>3</sub> 2 <sub>1</sub> 2
<i>a</i> , <i>b</i> , <i>c</i> (Å)	167.01, 167.01, 167.01	53.96, 53.96, 211.75	54.04, 54.04, 212.49
$\alpha$ , $\beta$ , $\gamma$ (°)	90, 90, 90	90, 90, 90	90, 90, 90
Resolution (Å)	47.21 – 2.00 (2.07– 2.00)	48.08 – 1.50 (1.53– 1.50)	48.17 – 1.50 (1.53 – 1.50)
<sup>a</sup> R <sub>sym</sub>	0.190 (4.101)	0.126 (4.893)	0.081 (3.670)
<sup>b</sup> R <sub>pim</sub>	0.030 (0.652)	0.018 (0.689)	0.017 (0.731)
<i>CC</i> <sub>1/2</sub>	1.00 (0.459)	0.991 (0.526)	0.999 (0.579)
<sup>c</sup> < <i>I</i> / $\sigma$ <i>I</i> >	20.7 (1.1)	24.6 (1.4)	17.5 (1.1)
Completeness	0.998 (0.973)	1.00 (1.00)	1.00 (1.00)
Redundancy	41.0 (38.5)	50.7 (51.0)	25.6 (26.0)
<b>Refinement</b>			
Resolution (Å)	20.00 – 2.00 (2.07– 2.00)	38.16 – 1.50 (1.55 – 1.50)	48.165 – 1.50 (1.55 – 1.50)
<sup>d</sup> R-work	0.1838 (0.300)	0.1702 (0.2740)	0.1817 (0.2938)
<sup>e</sup> R-free	0.21 (0.322)	0.1939 (0.3217)	0.2050 (0.2955)
RMS deviations in			
Bond lengths (Å)	0.002	0.012	0.005
Bond angles (°)	0.50	1.08	0.80
Chiral centers (Å <sup>3</sup> )	0.038	0.065	0.046
Planar groups (Å)	0.005	0.014	0.010
Estimated coordinate error (Å)	0.26	0.16	0.19
Ramachandran statistics (%)	98.95/1.05/0	98.63/1.37/0	98.63/1.37/0

<sup>a</sup>R<sub>sym</sub> =  $\sum_{hkl} \sum_i |I_i - \langle I \rangle| / \sum_{hkl} \sum_i I_i$  where *I<sub>i</sub>* is the *i*<sup>th</sup> measurement and  $\langle I \rangle$  is the weighted mean of all measurements of *I*.

<sup>b</sup>R<sub>pim</sub> =  $\sum_{hkl} 1 / (N-1)^{1/2} \sum_i |I_i(hkl) - \overline{I(hkl)}| / \sum_{hkl} \sum_i I_i(hkl)$ , where N is the redundancy of the data and  $\overline{I(hkl)}$  the average intensity.

<sup>c</sup><*I*/ $\sigma$ *I*> indicates the average of the intensity divided by its standard deviation.

<sup>d</sup>R<sub>work</sub> =  $\sum_{hkl} ||F_o| - |F_c|| / \sum_{hkl} |F_o|$  where *F<sub>o</sub>* and *F<sub>c</sub>* are the observed and calculated structure factor amplitudes.

<sup>e</sup>R<sub>free</sub> same as R for 5% of the data randomly omitted from the refinement. The number of reflections includes the R<sub>free</sub> subset.

Numbers in parentheses refer to the highest resolution data shell.

**Table 2.**

**Data Collection and Refinement Statistics.**

Ramachandran statistics reflect the percentage of residues in favored/allowed/outlier regions. **Source data** are available for this Table.

**Table 2.** (continued)

	7,8-DHF-mPDXP (+ P), protomer A	7,8-DHF-mPDXP (- P), protomer B
7,8-DHF-mPDXP (+ P), protomer B	0.43 Å	
Apo-mPDXP, protomer A	0.50 Å	0.71 Å
Apo-mPDXP, protomer B	0.60 Å	0.69 Å

	7,8-DHF-hPDXP (+ P)	7,8-DHF-hPDXP (- P)
7,8-DHF-hPDXP (- P)	0.37 Å	
Apo-hPDXP	0.54 Å	0.45 Å
PLP-hPDXP	0.39 Å	0.29 Å

$C\alpha$  atom-based alignment of the structures representing murine apo-PDXP (PDB: 4BX3), 7,8-DHF-bound murine PDXP (with inhibitor-bound protomer A and inhibitor-free protomer B; PDB: 8QFW), human apo-PDXP (PDB: 2P27), 7,8-DHF-bound human PDXP with phosphate (+ P) (PDB: 9EM1), 7,8-DHF-bound human PDXP without phosphate (- P) (PDB: 8S8A) and PLP-bound human PDXP (PDB: 2CFT); mPDXP, murine PDXP; hPDXP, human PDXP. Root mean square deviations are indicated.

**Table 3.**

**Alignment of murine and human PDXP structures.**

binding of the inhibitor, the side chain of Arg62 needs to adopt a completely extended conformation, which is prevented by the salt bridge. However, preventing mPDXP salt bridge formation by mutating Asp14 to Ala did not alter the efficacy of 7,8-DHF inhibition (**Fig. 3 – figure supplement 1d** [↗](#); see also **Fig. 3d** [↗](#) for the characterization of the PDXP-Arg62Ala variant). It is therefore currently unclear whether the mPDXP crystal state with only a single inhibitor bound per dimer reflects the state in solution. Due to the limited solubility of 7,8-DHF, we were unable to address the stoichiometry of 7,8-DHF binding to the PDXP dimer with isothermal calorimetry. It is conceivable that the mPDXP crystal packing is very stable (indeed, 7,8-DHF-bound mPDXP crystallized in the same cubic space group as apo-mPDXP, see ref. [\(48\)](#) [↗](#)), including the aforementioned salt bridge between Arg62 of the B-subunit and Asp14 of a symmetry-related molecule), and that the free energy generated by the formation of the crystal lattice is higher than the free energy generated upon inhibitor binding.

In contrast to murine PDXP, 7,8-DHF bound to human PDXP with a ratio of two inhibitors per homodimer (**Fig. 3a** [↗](#)) and well-defined density (**Fig. 3 – figure supplement 2a** [↗](#)). Interestingly, the orientation of the inhibitor was markedly affected by the presence or absence of phosphate (**Fig. 3b** [↗](#)). In the presence of phosphate, the inhibitor moiety that is closest to the  $Mg^{2+}$  cofactor is the uncharged phenyl ring of 7,8-DHF. In the absence of phosphate, the inhibitor is flipped horizontally, with the hydroxylated chromone substructure of 7,8-DHF now located closest to the  $Mg^{2+}$  ion (**Fig. 3b** [↗](#), compare *left* and *right panels*). The inhibitor localization in the presence of phosphate was identical in human and murine PDXP (**Fig. 3 – figure supplement 2e** [↗](#)). The localization of the phosphate ion that co-crystallized with 7,8-DHF-bound human or murine PDXP overlaps exactly with the localization of the PLP phosphate moiety introduced from PDB code 2CFT (human PDXP in complex with PLP) for visualization purposes (**Fig. 3c** [↗](#) and **Fig. 3 – figure supplement 2b** [↗](#)), indicating that the phosphate ion is bound in a catalytically relevant position.

Irrespective of the orientation of 7,8-DHF in the PDXP active site, the inhibitor is embedded in a cavity that is exclusively formed by the active site of protomer A, without a contribution of the dimerization interface with protomer B. All PDXP residues found to engage in 7,8-DHF interactions are identical in murine and human PDXP (**Fig. 3 – figure supplement 3** [↗](#)). One side of this cavity is formed by the more polar residues Asp27, Asn60, Ser61 and Arg62 (identical amino acid residue numbering in mPDXP and hPDXP), whereas the opposite side is established by the more hydrophobic residues Tyr150, His182, Pro183 and Leu184 (corresponding to Tyr146, His178, Pro179, and Leu180 in mPDXP). Adjacent to this hydrophobic stretch, the polar residue Glu152 (Glu148 in mPDXP) is located at the active site entrance, directly opposite of Arg62 on the more polar side of the 7,8-DHF binding channel (**Fig. 3b** [↗](#) and **Fig. 3 – figure supplement 1e** [↗](#)).

Interestingly, Glu152 (or Glu148) and Arg62 can form an intramolecular salt bridge that obstructs the active site entrance (**Fig. 3 – figure supplement 4** [↗](#)). This interaction was observed in phosphate-free 7,8-DHF-hPDXP and phosphate-free PLP-hPDXP, as well as in apo-hPDXP and apo-mPDXP. In contrast, the 7,8-DHF binding pose that is dictated by the concomitant binding of phosphate and 7,8-DHF interferes with the Glu152 (Glu148)-Arg62 interaction in both, hPDXP and mPDXP (**Fig. 3 – figure supplement 4** [↗](#)). Thus, although we did not find evidence for major cap/core or substrate-specificity loop movements ([40](#) [↗](#), [48](#) [↗](#)) in PDXP, the presence or absence of a salt bridge formed between the cap domain residue Glu152 (Glu148) and the core domain residue Arg62 indicates subtle conformational changes in PDXP that may mediate an opening or a closure of the active site entrance.

Inhibitor binding in the presence of phosphate is identical in human and murine PDXP (**Fig. 3 – figure supplement 1f** [↗](#)) and appears to be primarily stabilized by two hydrogen bonds, as well as polar and non-polar interactions (**Fig. 3b** [↗](#), *left panel*). The side chain hydroxyl group of Ser61 forms a direct hydrogen bond with the ketone group of the inhibitor, which is additionally coordinated by the Ser61 backbone nitrogen atom. Furthermore, Glu152 (Glu148) forms a direct hydrogen bond via its carboxylic acid with the 7-hydroxyl group of 7,8-DHF. The side chains of the

polar residues Asp27, Asn60 and Arg62 engage in van der Waals interactions with 7,8-DHF. The two hydroxyl groups of the 7,8-DHF benzyl ring engage in van der Waals interactions with the guanidinium group of Arg62 and the carboxylic acid function of Glu148 (Glu152). On the more hydrophobic side of the binding cavity, Tyr146 (Tyr150) forms  $\pi$ -electron stacking interactions with the pyrone ring of 7,8-DHF. In addition, the His178 (His182) imidazole group coordinates the 7,8-DHF phenyl ring via a cation- $\pi$  interaction. His178 (His182), located in the substrate specificity loop, and Asn60 and Arg62 are also important for PLP binding (48, 49).

Inhibitor binding in the absence of phosphate is primarily stabilized by metal coordination and hydrogen bonds, as well as polar and non-polar interactions (Fig. 3b, right panel). The 7-hydroxyl group of 7,8-DHF is involved in an octahedral  $Mg^{2+}$  coordination, albeit with an elongated oxygen- $Mg^{2+}$  distance of 2.7 Å, leading to the displacement of a water molecule (Fig. 3c). This inhibitor-based water displacement is not observed in the phosphate-containing murine or human 7,8-DHF-PDXP structures. The 8-hydroxyl group of 7,8-DHF forms a hydrogen bond with Asp239 and His182. The ketone group of the inhibitor participates in a water-bridged hydrogen bond to the carboxyl group of Asp27 and the backbone amine group of Gly33. Like in the phosphate-containing structure, the His182 imidazole group coordinates the 7,8-DHF phenyl ring via  $\pi$ - $\pi$  stacking. In addition, Tyr150 forms edge to face  $\pi$ - $\pi$  stacking interactions with the phenyl ring of 7,8-DHF. The side chains of the polar residues Asp27, Asn60, and, to some degree, also of Arg62, engage in van der Waals interactions with 7,8-DHF.

To verify the putative 7,8-DHF – PDXP interactions, we introduced single mutations into the binding interface. Asn60, Arg62, Tyr146, Glu148 and His178 in mPDXP were each exchanged for Ala (PDXP<sup>N60A</sup>, PDXP<sup>R62A</sup>, PDXP<sup>Y146A</sup>, PDXP<sup>E148A</sup>, or PDXP<sup>H178A</sup>, respectively). Since the carboxamide group of Asn60 can form a hydrogen bond with the carboxylate moiety of Asp27, and a loss of this interaction in the PDXP<sup>N60A</sup> variant is predicted to alter the PDXP structure, we additionally mutated Asn60 to Ser (PDXP<sup>N60S</sup>). PDXP variants were recombinantly expressed and purified from *E. coli* (see Fig. 3 – figure supplement 5 for protein purity). Figure 3d (left panel) shows that all PDXP variants were enzymatically active. As expected, the phosphatase activities of PDXP<sup>N60A</sup> and of PDXP<sup>H178A</sup> were reduced. The somewhat elevated phosphatase activity of PDXP<sup>Y146A</sup> and PDXP<sup>E148A</sup> is currently unexplained. Importantly, all variants except PDXP<sup>N60A</sup> and PDXP<sup>N60S</sup> were resistant to 7,8-DHF, supporting the essential role of each of these residues for inhibitor binding and the minor contribution of the weak van der Waals interactions between Asn60 and 7,8-DHF during inhibitor binding (Fig. 3d, right panel). These data also suggest that Asn61 contributes to the limited efficacy of 7,8-mediated PDXP inhibition in vitro.

Based on the inhibitor-bound structures and the predominantly competitive component of PDXP inhibition by 7,8-DHF (increased  $K_M$ , see Table 1), it seems likely that 7,8-DHF sterically hinders substrate access to the active site, and competes with PLP coordination (Fig. 3 – figure supplement 2b). In addition, BLI measurements (see Fig. 2c) showed a relatively slow association rate and extended residence time of 7,8-DHF ( $\tau=30.3$  s). This may indicate a reorganization of the  $Mg^{2+}$ -coordination due to inhibitor binding, and a reorientation of 7,8-DHF during the PDXP catalytic cycle. The reduced rate of product formation may account for the apparent mixed mode of 7,8-DHF-mediated PDXP inhibition (reduction of  $v_{max}$ , see Table 1).

## 7,8-DHF functions as a PDXP inhibitor in hippocampal neurons

To investigate cellular target engagement of 7,8-DHF, we isolated primary hippocampal neurons from PDXP-WT and PDXP-KO embryos. PDXP deficiency increased total PLP levels 2.4-fold compared to PDXP-WT neurons (Fig. 4a). This finding is in good agreement with the PLP increase resulting from PDXP loss in total hippocampal extracts (see Fig. 1). The larger absolute PLP values in cultured neurons are likely attributable to the high concentration of the PLP precursor pyridoxal (20  $\mu$ M) in the culture medium. We did not observe PDXP-dependent changes

in pyridoxal kinase (PDXK) expression (**Fig. 4b**) and could not detect pyridox(am)ine-5'-phosphate oxidase (PNPO) in hippocampal neuronal cultures, suggesting that the PLP increase was primarily caused by the constitutive PDXP loss.

To assess the consequences of 7,8-DHF treatment on PLP levels in hippocampal neurons, we chose short-term incubation conditions (45 min, 20  $\mu$ M) to avoid possible secondary effects of the inhibitor. As expected, the acute effect of 7,8-DHF treatment in WT cells was much more subtle ( $\sim$ 9% increase in total PLP) than the impact of long-term PDXP-deficiency ( $441.3 \pm 62.6$  nmol PLP/g protein in DMSO solvent control-treated cells versus  $482.7 \pm 130.4$  nmol PLP/g protein in 7,8-DHF treated cells; data are mean values  $\pm$  S.E. of  $n=4$  independent experiments). However, this effect is likely underestimated because only the PDXP-accessible pool of non-protein-bound PLP may be impacted by 7,8-DHF (see **Fig. 1c**). Due to the limited number of available hippocampal neurons, we were unfortunately unable to obtain sufficient quantities of protein-depleted PLP pools to address this question.

Acute changes in the PLP/PL ratio may be a more sensitive indicator of PDXP activity than changes in total PLP levels alone, because PDXP inhibition is expected to increase cellular levels of PLP (the PDXP substrate) and to concomitantly decrease the levels of PL (the product of PDXP phosphatase activity). The PLP/PL ratio is also independent of the exact protein concentration in a given extract of hippocampal neurons, thus optimizing comparability between samples. As shown in **Fig. 4c**, 7,8-DHF significantly increased the PLP/PL ratio in PDXP-WT, but not in PDXP-KO hippocampal neurons (+18% versus +1% compared to the respective DMSO controls). Together, these data indicate that 7,8-DHF can modulate cellular PLP levels in a PDXP-dependent manner and validate PDXP as a 7,8-DHF target in primary hippocampal neurons.

## Discussion

PLP deficiency has been associated with human brain disorders for decades (3), yet causal links remain unclear. Aside from vitamin B6 administration, pharmacological strategies to elevate intracellular PLP levels are lacking. Here, we identify 7,8-dihydroxyflavone (7,8-DHF) as a direct PDXP inhibitor that increases PLP levels in hippocampal neurons, validating PDXP as a druggable target to control intracellular PLP levels in the brain. We also present three high-resolution 7,8-DHF/PDXP co-crystal structures that will facilitate the design of more potent, efficacious, and selective PDXP inhibitors in the future. Such molecules might improve the control of intracellular PLP levels and help to elucidate a possible contribution of PLP to the pathophysiology of brain disorders. Our observation that the expression of PDXP is substantially upregulated in hippocampi of middle-aged mice suggests that a therapeutic vitamin B6 supplementation alone may not suffice to elevate intracellular PLP levels under conditions where the PLP-degrading phosphatase is hyperactive.

The discovery of 7,8-DHF as a direct PDXP inhibitor was unexpected. Interestingly, numerous *in vivo* studies have reported the effectiveness of 7,8-DHF in brain disorder models, including rodent models of Alzheimer's disease (50–57), depression (58–63), schizophrenia (64–68), epilepsy (69, 70) and autism (71–74). Although PLP deficiency is thought to contribute to the respective human conditions (3, 75, 76), PLP-dependent processes have not yet been considered in the context of 7,8-DHF-induced effects.

7,8-DHF was initially discovered as a small-molecule TrkB agonist with BDNF-mimetic activity (77). BDNF, a high-affinity TrkB ligand, is an important neuropeptide for nervous system function and pathology. Consensus is emerging that BDNF plays a key role in the treatment response to neuropsychiatric drugs (32). Therapeutics that target BDNF/TrkB-signaling are thus of interest as disease-modifying agents in several brain disorders. Since BDNF does not cross the blood-brain barrier, attempts have been made to develop small molecule BDNF mimetics. Several

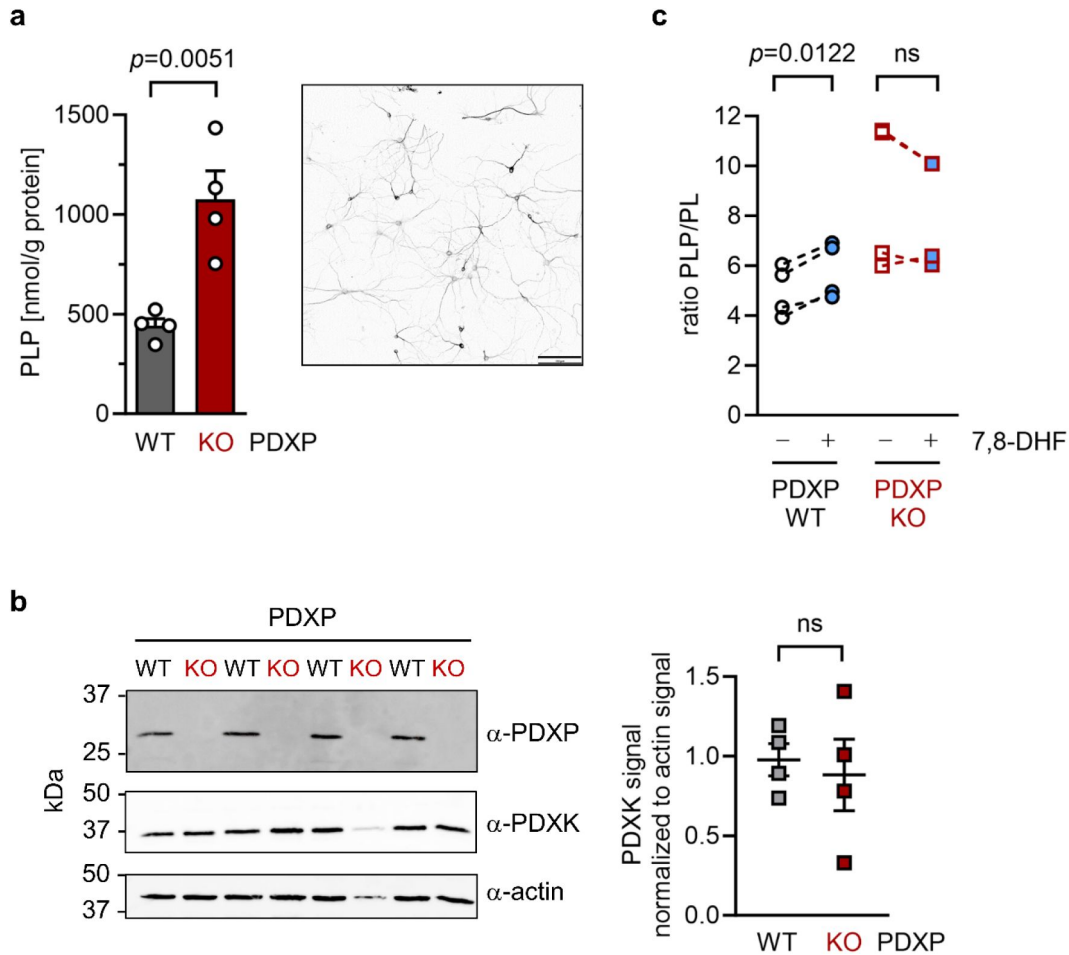


**Figure 4.**

**Effect of 7,8-DHF on the PLP/PL ratio in cultured hippocampal neurons from WT or PDXP-KO mice.**

(a) Effect of long-term PDXP deficiency on total PLP levels in hippocampal neurons. Data are mean values  $\pm$  S.E. of  $n=4$  independent experiments. Statistical significance was assessed with a two-tailed, unpaired *t*-test. A representative image of primary hippocampal neurons stained for the neuronal marker protein MAP2 is shown in the insert (pixel intensities were color-inverted for better visualization). Scale bar, 100  $\mu$ m. (b) Western blot analysis of PDXP and PDXK expression in hippocampal neuron samples shown in (a). The same blots were reprobed with  $\alpha$ -actin antibodies as a loading control. The densitometric quantification of PDXK signals is shown on the right; data are mean values  $\pm$  S.E. of  $n=4$  independent experiments. (c) Effect of 7,8-DHF (20  $\mu$ M, 45 min) or the DMSO solvent control (0.02% v/v, 45 min) on the PLP/PL ratio in hippocampal neurons of PDXP-WT or PDXP-KO mice. **Source data** are available for this Figure.

candidates have been reported, including 7,8-DHF (33 [↗](#), 77 [↗](#)). Nevertheless, the on-target selectivity and efficacy of these compounds is actively debated. Using quantitative and direct assays to measure TrkB dimerization and activation, TrkB downstream signaling pathways, TrkB-dependent gene expression and cytoprotection, 7,8-DHF and other reported small-molecule TrkB agonists failed to activate TrkB in cells (33 [↗](#)–35 [↗](#)). An electrophysiological study in acute hippocampal slice preparations demonstrated that 7,8-DHF potentiates hippocampal mossy fiber-CA3 synaptic transmission in a TrkB receptor-independent manner (78 [↗](#)). Overall, it appears that the mechanism of action of 7,8-DHF is incompletely understood, but 7,8-DHF targets other than TrkB so far have remained elusive. The identification of 7,8-DHF as a PDXP inhibitor reported here indicates that this flavone may modulate vitamin B6-dependent processes and suggests that PDXP could be explored as a pharmacological entry point into brain disorders.

## Materials and methods

### Materials

Unless otherwise specified, all reagents were of the highest available purity and purchased from Sigma Aldrich (Schnelldorf, Germany). 3,7,8,4'-Tetrahydroxyflavone was obtained from Ambinter (Orléans, France), all other flavones were from Sigma Aldrich.

### PDXP knockout mice

Floxed PDXP mice (*Pdpx<sup>tm1Goh</sup>*) were generated on a C57Bl/6J background, and whole-body *Pdpx* knockouts were achieved by breeding with B6.FVB-Tg(EIIa-cre)C5379Lmgd/J (EIIa-Cre) transgenic mice, as described (30 [↗](#)). All experiments were authorized by the local veterinary authority and committee on the ethics of animal experiments (Regierung von Unterfranken). All analyses were carried out in strict accordance with all German and European Union applicable laws and regulations concerning care and use of laboratory animals.

### Preparation of hippocampi and hippocampal neurons and immunocytochemistry

Mice were sacrificed by cervical dislocation, and brains were immediately placed on a pre-cooled metal plate and dissected under a Leica M80 binocular (Leica, Wetzlar, Germany). Hippocampi were weighed and flash-frozen in liquid nitrogen. The entire procedure was performed in <3 min. Hippocampal lysates were prepared by the addition of ice-cold PBS (200  $\mu$ L PBS/10 mg hippocampal wet weight) and homogenized for 1 min in a TissueLyser II instrument (Qiagen, Hilden, Germany). One fourth of the obtained volume of each lysate was used for the analysis of total PLP concentrations as described below. To determine protein-depleted PLP (27 [↗](#)), the remaining volume of each lysate was centrifuged at  $14,000 \times g$  for 15 min at 4°C. The supernatant was applied to 3 kDa MWCO filters (Amicon Ultra-0.5 Centrifugal Filter; Merck Millipore, Darmstadt, Germany), and centrifuged at  $14,000 \times g$  for 45 min at 4°C. The flow-through was collected and prepared for HPLC analysis (see below).

Primary hippocampal neuronal cultures were prepared from mouse embryos at embryonic day 17. Hippocampi were incubated with 0.5 mg/mL trypsin, 0.2 mg/mL EDTA and 10  $\mu$ g/mL DNase I in PBS for 30 min at 37°C. Trypsinization was stopped by adding 10% fetal calf serum. Cells were dissociated by trituration, counted, and seeded at a density of 150,000 cells per 35 mm dish. Dissociated cells were grown in neurobasal medium supplemented with L-glutamine and B27 supplement (A3582801, Life Technologies, Dreieich, Germany) with an exchange of 50% of the medium after 6 days in culture. After 21 days of differentiation (day in vitro 21/DIV21), 7,8-DHF (20  $\mu$ M) or DMSO (0.02%, v/v) was added to the hippocampal neuronal cultures for 45 min. Cells were rinsed once with PBS (37°C), lysed in 150  $\mu$ L ice cold H<sub>2</sub>O, and placed at -80°C for at least 30 min.



For immunocytochemistry, DIV21 primary hippocampal neurons were fixed with 4% (w/v) paraformaldehyde in phosphate-buffered saline (PBS) for 15 min at RT. After washing twice with PBS, 50 mM  $\text{NH}_4\text{Cl}$  was added for 10 min. Cells were then permeabilized with 0.1% (v/v) Triton X-100 and blocked with 5% (v/v) goat serum in PBS for 30 min at 22°C. Cells were incubated with mouse monoclonal anti-MAP2 antibodies (1:500 dilution, clone MAB3418, Millipore, Darmstadt, Germany) for 1 h in 5% goat serum/PBS at 22°C. Alexa-488-labeled secondary goat anti-mouse antibodies (1:500 dilution; Dianova, Hamburg, Germany) were applied for 1 h. Nuclei were counter-stained with 4',6-diamino-2-phenylindole (DAPI), and slides were mounted with Mowiol. Images were acquired using an inverted IX81 microscope equipped with an Olympus UPLSAPO 60× oil objective (numerical aperture: 1.35) on an Olympus FV1000 confocal laser scanning system, using a FVD10 SPD spectral detector and diode lasers of 405 nm (DAPI) and 495 nm (Alexa488).

## Determination of PLP and PL by high-performance liquid chromatography (HPLC)

Samples were derivatized as described (79). Briefly, 100  $\mu\text{L}$  of lysate were mixed with 8  $\mu\text{L}$  derivatization agent (containing 250 mg/mL of both semicarbazide and glycine), and incubated on ice for 30 min. Samples were then deproteinized by addition of perchloric acid (8  $\mu\text{L}$  of a 72% (w/v) stock solution), followed by centrifugation at  $15,000 \times g$  for 15 min at 4 °C. Supernatants (100  $\mu\text{L}$ ) were neutralized with 10  $\mu\text{L}$  NaOH (25% (v/v) stock solution), and 2  $\mu\text{M}$  pyridoxic acid was added as an internal standard. PLP and PL were subjected to the same derivatization protocol to establish a standard curve. Samples were analyzed on a Dionex Ultimate 3000 HPLC (Thermo Fisher Scientific, Dreieich, Germany), using 60 mM  $\text{Na}_2\text{HPO}_4$ , 1 mM EDTA, 9.5% (v/v) MeOH; pH 6.5 as mobile phase. PL, PLP and pyridoxic acid were separated on a 3  $\mu\text{m}$  reverse phase column (BDS-HYPERSIL-C18, Thermo Fisher Scientific). Chromatograms were analyzed using Chromeleon 7 software (Thermo Fisher Scientific).

## Western blotting

Tissue or cell homogenates (prepared as detailed above for HPLC analysis) were extracted with 4 × RIPA buffer (final concentration, 50 mM Tris, pH 7.5; 150 mM NaCl, 1% (v/v) Triton X-100, 0.5% (v/v) sodium deoxycholate, 0.1% (w/v) SDS, 1 mM 4-(2-aminoethyl)benzenesulfonyl fluoride (Pefabloc), 5  $\mu\text{g}/\text{mL}$  aprotinin, 1  $\mu\text{g}/\text{mL}$  leupeptin, 1  $\mu\text{g}/\text{mL}$  pepstatin) for 15 min at 4 °C under rotation, and lysates were clarified by centrifugation ( $20,000 \times g$ , 15 min, 4 °C). Protein concentrations in the supernatants were determined using the Micro BCA Protein Assay Kit (Thermo Fisher Scientific). Proteins were separated by SDS-PAGE and transferred to nitrocellulose membranes by semidry-blotting. Antibodies were purchased from the following providers: Merck Millipore (mouse monoclonal  $\alpha$ -actin mAb1501, dilution 1:5000); Cell Signaling (rabbit monoclonal  $\alpha$ -PDXP clone C85E3, dilution 1:1000; Cell Signaling, Danvers/Massachusetts, USA), Sigma Aldrich (rabbit polyclonal  $\alpha$ -PDXK/AB1, #AV53615, dilution 1:1000), and Thermo Fisher Scientific (rabbit polyclonal  $\alpha$ -PNPO, #PA5-26400, dilution 1:1000, as used in ref. (30)). Western blots were densitometrically quantified with NIH ImageJ, version 1.45i.

## Phosphatase plasmids and cloning

N-terminally GST-tagged, human PDXP was in pGEX-4T-1 (Amersham Biosciences, Amersham, UK). N-terminally His<sub>6</sub>-SUMO-tagged human PDXP was cloned into pET-SUMO (coding for human SUMO; a kind gift of Dr. Pedro Friedmann Angeli, Rudolf-Virchow-Center, University of Würzburg, Germany); His<sub>6</sub>-SenP2 (EMBL Heidelberg) was in pET-M11. All other phosphatases were of murine origin and were subcloned into pET-M11 (EMBL), as described (40). *Pdxp* point mutants (generated by nested PCR) were subcloned into the *NcoI* (*PciI* for *PspH*) and *EcoRI* restriction sites of pET-M11, using Q5 Hot Start High-Fidelity DNA Polymerase (New England Biolabs, Frankfurt/Main, Germany). *Pdxp-D14N* was generated with the Platinum SuperFi II DNA

Polymerase Mastermix according to mutagenesis protocol A provided by the manufacturer (Thermo Fisher Scientific) and cloned into pET-M11 as described above. The following primers (oligonucleotide sequence 5'-3'; fwd, forward; rev, reverse) were used:

*Pdyp* fwd: TCGACCATGGCGCGCTGCGAGCGG  
rev: AAAAGTGAATTCTCAGTCCTCCAGCCCCCTC

*Pdyp-D14A* fwd: GCCCTGCGCGCCGTGCTGGGCCAGGCGCAG  
rev: GCCCAGCACGGCGCGCAGGGCCGCGCCGCG

*Pdyp-N60A* fwd: TTCGTGAGCAACGCCAGCCGGCGCGCG  
rev: CGCGCGCCGGCTGGCGTTGCTCACGAA

*Pdyp-N60S* fwd: TTCGTGAGCAACAGCAGCCGGCGCGCG  
rev: CGCGCGCCGGCTGCTGTTGCTCACGAA

*Pdyp-R62A* fwd: AGCAACAACAGCGCGCGCGCGCGGCCC  
rev: GGGCCGCGCGCGCGCGCTGTTGTTGCT

*Pdyp-Y146A* fwd: GTGCTCGTAGGCGCCGACGAGCAGTTT  
rev: AAAGTCTCGTCGGCGCCTACGAGCAC

*Pdyp-E148A* fwd: GTAGGCTACGACGCGCAGTTTTTCCTTC  
rev: GAAGGAAAAGTCTGCGCGTCGTAGCCTAC

*Pdyp-H178A* fwd: CGCGACCCTTGGGCCCCGCTCAGCGAC  
rev: GTCGCTGAGCGGGGCCCAAGGGTCGCG

Primers were purchased from Eurofins Genomics (Ebersberg, Germany), and all constructs were verified by sequencing (Microsynth Seqlab, Göttingen, Germany).

### Expression and purification of recombinant proteins

Human His<sub>6</sub>-SUMO-tagged PDXP was grown in ZYP-5052 autoinduction medium for 7 h at 37° C, followed by 48 h at 21°C (80%). All purification steps of murine PDXP and murine PGP were carried out exactly as described (40%). The purification of the His<sub>6</sub>-SUMO-tagged human PDXP was carried out exactly as described for murine His<sub>6</sub>-tagged PDXP (40%), except that human SenP2 protease was used to cleave the His<sub>6</sub>-SUMO-tag. N-terminally His<sub>6</sub>-tagged PDXP variants and

His<sub>6</sub>-SenP2 were expressed as described for PDXP-WT (40). With the exception of PDXP-D14, the His<sub>6</sub>-tag was not cleaved off. Human GST-PDXP was transformed into *E. coli* BL21(DE3) (Stratagene Europe/VWR, Darmstadt, Germany). Protein expression was induced with 0.5 mM isopropyl β-d-thiogalactopyranoside for 18 h at 20 °C. All subsequent purification steps were carried out at 4 °C. Cells were harvested by centrifugation for 10 min at 8000 × *g* and resuspended in lysis buffer (100 mM triethanolamine/TEA, 500 mM NaCl; pH 7.4) supplemented with protease inhibitors (EDTA-free protease inhibitor tablets; Roche, Mannheim, Germany) and 150 U/mL DNase I (Applichem, Renningen, Germany). Cells were lysed using a cell disruptor (Constant Systems, Daventry, UK), and cell debris was removed by centrifugation for 30 min at 30,000 × *g*. GST-PDXP was batch-purified on a glutathione sepharose 4B resin (GE Healthcare, Uppsala, Sweden). After extensive washing with 25 column volumes of wash buffer (50 mM TEA, 250 mM NaCl; pH 7.4), GST-PDXP was eluted in wash buffer supplemented with 10 mM reduced glutathione, concentrated, and further purified in buffer A (50 mM TEA, 250 mM NaCl, 5 mM MgCl<sub>2</sub>; pH 7.4) using a HiLoad 16/60 Superdex 200 pg gel filtration column operated on an ÄKTA liquid chromatography system (GE Healthcare).

## High-Throughput Screen for PDXP Modulators

The screening campaign (chemical library, screening protocol, concentration-dependent assays, data analysis) was conducted exactly as described previously (40), except that the primary screen was done with PDXP, the counter-screen with PGP, and PDXP inhibitor hits were validated using 5'-pyridoxal phosphate (PLP) as a physiological PDXP substrate.

## IC<sub>50</sub> determinations, enzyme kinetics, and compound selectivity

Conditions for enzymatic assays were as previously published (40), with the following modifications. Bovine brain calcineurin (PP2B, Sigma Aldrich #C1907) activity against the PKA regulatory subunit type II (phosphopeptide DLDVPIPIGRFDRRVpSVAAE; Sigma Aldrich #207008) was assayed at 37°C in 100 mM NaCl, 50 mM Tris, 6 mM MgCl<sub>2</sub>, 0.5 mM CaCl<sub>2</sub>, 0.5 mM DTT, 0.025% (v/v) NP40; pH 7.5. Recombinant human PTP1B (amino acids 1-321, Cayman Chemical, Ann Arbor, Michigan, USA) activity against the Tyr<sup>992</sup> autophosphorylation site of EGFR (DADEpYLIPQQG; Santa Cruz Biotechnology, Heidelberg, Germany) was assayed at 30°C in 150 mM NaCl, 50 mM 2-(N-morpholino)ethanesulfonic acid, 1 mM EDTA; pH 7.2. Murine PDXP-D14A was assayed exactly like PDXP-WT in 30 mM triethanolamine, 5 mM MgCl<sub>2</sub>, 30 mM NaCl; pH 7.5, supplemented with 0.01% (v/v) Triton X-100.

Flavone stocks were prepared at 10 mM in 100% DMSO. A constant final DMSO concentration of 0.4% was maintained under all conditions, and solvent control samples contained 0.4% DMSO without compounds. Purified phosphatases were pre-incubated for 10 min at RT with serial dilutions of flavones. Dephosphorylation reactions were started by the addition of the indicated substrate; buffer with substrate and the respective flavone but without the enzyme served as a background control. Prior to compound testing, time courses of inorganic phosphate release from the respective phosphatase substrates were conducted to ensure assay linearity. Inorganic phosphate release was detected with a malachite green solution (Biomol Green; Enzo Life Sciences, Lörrach, Germany); the absorbance at 620 nm ( $A_{620}$ ) was measured on an Envision 2104 multilabel reader (Perkin Elmer, Rodgau, Germany). Released phosphate was determined by converting the values to nmol P<sub>i</sub> with a phosphate standard curve. Data were analyzed with GraphPad Prism version 9.5.1 (GraphPad, Boston/Massachusetts, USA). For IC<sub>50</sub> determinations, log<sub>inhibitor</sub> versus response was calculated (four parameter). To derive K<sub>M</sub> and k<sub>cat</sub> values, data were fitted by nonlinear regression to the Michaelis-Menten equation.

## Biolayer interferometry (BLI)

PDXP was biotinylated using the EZ-Link NHS-PEG4-Biotin kit, as recommended by the manufacturer (Thermo Fisher Scientific), and loaded on Super Streptavidin Biosensors (SSA) (Sartorius, Göttingen, Germany) as follows. SSA sensors were equilibrated for 1 h at RT in BLI assay buffer (250 mM triethanolamine, 5 mM MgCl<sub>2</sub>, 250 mM NaCl, 0.005% (v/v) TWEEN-20; pH 7.5), loaded with 200 µg/mL biotinylated PDXP, blocked with 2 µg/mL biocytin, and washed in BLI assay buffer. Reference SSA sensors were blocked with 2 µg/mL biocytin (81 [↗](#)). Six point 1:1 serial dilution series of 7,8-DHF and 5,7-DHF were prepared in DMSO, and BLI assay buffer was added to the wells to obtain a 7,8-DHF starting concentration of 25 µM. The final DMSO concentration was 5% (v/v). Buffers for baseline, dissociation, and buffer correction wells were supplemented with the same amount of DMSO for identical buffer conditions. Four measurements were carried out per condition, using one sensor set for two measurements. All measurements were conducted on an Octet K2 device (Sartorius) using 96-well plates. Assay settings were as follows: baseline measurement 45 sec, association time 90 sec, dissociation time 150 sec. The resulting data were processed using the double reference method of the Octet analysis software for removal of drifts and well-to-well artefacts. Kinetic analyses were performed using the Octet analysis software. The steady state analysis was carried out with OriginPro 2021b (OriginLab, Northampton/Massachusetts, USA), using a dose-response model for regression. Due to the poor solubility of 7,8-DHF, the highest concentration of 25 µM was not included in the analysis.

## PDXP crystallization and data collection

For co-crystallization with 7,8-DHF, full-length murine PDXP (10 mg/mL in 50 mM triethanolamine; 250 mM NaCl; 5 mM MgCl<sub>2</sub>; pH 7.4) was supplemented with a three-fold molar excess of the flavone. Prism-shaped crystals of 7,8-DHF-bound murine PDXP were grown at 20°C in 0.1 M phosphate citrate (pH 4.2) and 40% (v/v) PEG 300 using the sitting-drop vapor diffusion method. Human PDXP crystals were grown at 20 °C in 0.1 M Tris (pH 8.5) and 1 M diammonium hydrogen phosphate, or in 0.1 M HEPES (pH 7.0), 15% (v/v) Tacsimat pH 7.0 (Hampton Research, Aliso Viejo, USA) and 2% (w/v) PEG 3350 using the sitting-drop vapor diffusion method. Crystals were cryoprotected for flash-cooling in liquid nitrogen by soaking in mother liquor containing 25% (v/v) glycerol. Diffraction data of murine PDXP in complex with 7,8-DHF were collected from flash-cooled crystals at a temperature of 100 K on beamline BL 14.1 at the BESSY synchrotron (Helmholtz Zentrum Berlin, Germany). Diffraction data of 7,8-DHF bound to human PDXP were collected on beamline ID23-2 at the ESRF (Grenoble, France) [<https://data.esrf.fr/doi/10.15151/ESRF-ES-1409594895> [↗](#)]. Diffraction data were processed using XDS (82 [↗](#)) and further analysed with Aimless (83 [↗](#)) of the CCP4 suite (84 [↗](#)). The structures of 7,8-DHF-PDXP were solved by molecular replacement with the program Phaser (85 [↗](#)) with the structure of the murine PDXP (PDB entry 4BX3) or human PDXP (PDB entry 2P27) as search models, and refined with Phenix (86 [↗](#)). Model building was carried out in COOT (87 [↗](#)). Structural illustrations were prepared with PyMOL 2.5.1 (88 [↗](#)).

## Acknowledgements

We thank Carola Seyffarth and Nicole Bader for excellent technical assistance, Dr. Jochen Kuper for collecting the murine PDXP diffraction data, the staff at beamline BL14.1 of the BESSY synchrotron, and the staff at beamline ID23-2 of the ESRF synchrotron for technical support. A part of this work was initially funded by the DFG Collaborative Research Center SFB688 (TP A11 to A.G.).

## Data availability statement

The previously published PDB entry 4BX3 of murine apo-PDXP [<http://doi.org/10.2210/pdb4BX3/pdb>], 2P27 of human apo-PDXP [<http://doi.org/10.2210/pdb2P27/pdb>] and 2CFT of PLP-bound human PDXP [<http://doi.org/10.2210/pdb2CFT/pdb>] are used in this manuscript. X-ray crystallographic data of 7,8-DHF-bound murine PDXP generated in this study have been deposited in the PDB and can be accessed under the PDB entry 8QFW [<http://doi.org/10.2210/pdb8QFW/pdb>]. X-ray crystallographic data of 7,8-DHF-bound human PDXP generated in this study can be accessed under the PDB entries 8S8A (without phosphate) [<http://doi.org/10.2210/pdb8S8A/pdb>] and 9EM1 (with phosphate) [<http://doi.org/10.2210/pdb9EM1/pdb>]. The corresponding raw diffraction images have been deposited in the Xtal Raw Data Archive and can be accessed under the XRDA entries 8QFW [<https://xrda.pdbj.org/entry/8qfw>], 8S8A [<https://xrda.pdbj.org/entry/8s8a>], and 9EM1 [<https://xrda.pdbj.org/entry/9em1>].

## Author contributions

Conceptualization, A.G.; validation, E.J.; formal analysis, M.B., C.Z., L.W., S.B., M.N., H.S., E.J., A.G.; investigation, M.B., C.Z., L.W., A.K., K.H., S.B., M.N., E.J.; resources, C.V., M.N., J.P.v.K., H.S.; writing – original draft preparation, A.G. with input from E.J. and H.S.; writing – revised manuscript: A.G. and M.B. with input from H.S. and S.B.; visualization, M.B., C.Z., L.W., S.B., E.J., A.G.; supervision, E.J., A.G.; project administration, A.G.; funding acquisition, A.G.

## Competing interests

A.G. is a recipient of a research project grant from Boehringer Ingelheim International GmbH. This project funding is independent of and has no overlap with the work described in this manuscript. The other authors declare no competing interests.

## Supplementary information

PDXP-WT		PDXP-KO	
age [days]	PLP [nmol/g protein]	age [days]	PLP [nmol/g protein]
18	66.77	18	<b>154.60</b>
18	<b>111.66</b>	18	<b>144.50</b>
18	<b>110.11</b>	18	<b>154.74</b>
39	<b>99.73</b>	34	<b>169.06</b>
39	107.59	34	<b>177.57</b>
39	109.60	40	153.93
42	89.62	41	<b>180.65</b>
42	<b>105.82</b>	41	157.84
42	<b>104.38</b>	41	166.67
59	71.55	60	180.58
59	68.99	60	142.33
84	59.36	87	214.52
84	65.52	87	198.61
86	73.50	94	196.21
86	74.40	94	211.20
94	123.81	94	214.70
94	116.81	94	201.21
94	138.95	94	230.42
136	84.61	142	192.13
176	72.22	142	188.03
176	72.83	162	143.41
252	<b>83.47</b>	162	158.23
252	<b>85.78</b>	256	<b>180.26</b>
252	<b>78.88</b>	256	<b>184.36</b>
252	72.86	256	<b>168.17</b>
252	62.20	256	191.69
252	69.15	256	182.87
269	72.53	256	189.11
269	90.90	327	149.04
269	80.60	327	139.20
335	52.90	351	165.84
335	<b>60.93</b>	351	<b>163.33</b>
335	<b>52.17</b>	351	<b>142.23</b>
335	<b>65.93</b>	351	<b>155.71</b>
		366	156.26

Figure 1 – figure supplement 1.

#### Analysis of total hippocampal PLP levels in PDXP-WT and PDXP-KO mice.

Each value represents the result of the PLP determination in an individual hippocampus. Analysis for statistically significant differences between PLP levels in PDXP-WT and PDXP-KO hippocampi (all ages combined; two-tailed, unpaired *t*-test)  $p < 0.0001$ . Bold table entries indicate those hippocampal extracts that were further separated for an analysis of protein-depleted and protein-bound PLP (see Fig. 1c). Source data are available for this Table.

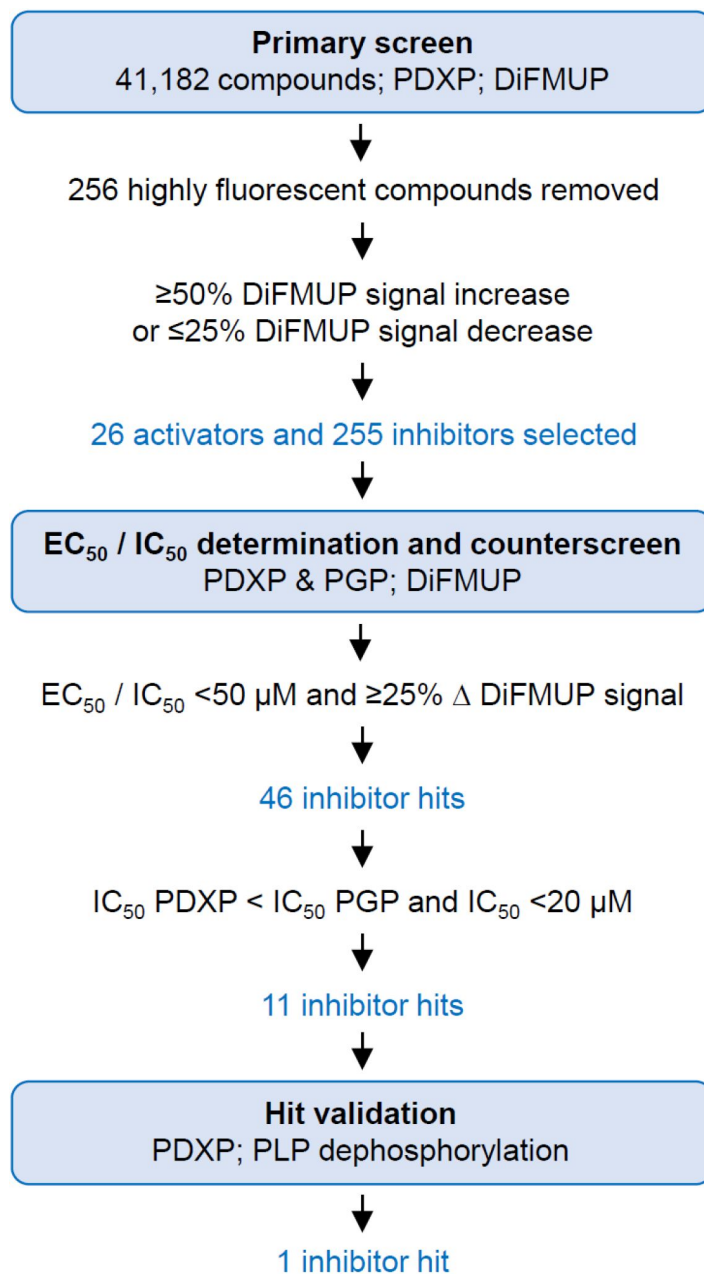


**Figure 2 – figure supplement 1.**

#### **Identification of PDXP inhibitors.**

A primary screen was conducted using 6,8-difluoro-4-methylumbelliferyl phosphate (DiFMUP) as an artificial substrate. Out of 41,182 screened compounds, 256 compounds were discarded that showed very high autofluorescence (as recognized by elevated fluorescence at the start of the kinetic curve); 26 compounds showed statistically significant PDXP activation, and 255 compounds showed PDXP inhibition (as recognized by an elevated or decreased slope of the kinetic curve, respectively). The average Z'-factor of the screen was  $0.75 \pm 0.112$ . These 281 compounds were selected for DiFMUP-based concentration-dependent validation, and the 46 most potent compounds were selected. A counter-screening was conducted in parallel, also in a concentration-dependent fashion, against the PDXP paralog and closest relative phosphoglycolate phosphatase (PGP). The 11 compounds that were inactive against PGP were validated in a secondary assay, using the PDXP substrate pyridoxal 5'-phosphate (PLP). One PDXP inhibitor hit blocked PLP dephosphorylation by  $\geq 50\%$ . **Source data** are available for this Figure.

	<b>InChI Key</b>	<b>IC<sub>50</sub> [μM]</b>
7,8-DHF	COCYGNDCWFKTMF-UHFFFAOYSA-N	0.8 *
	RDMYXZLESVAHOO-UHFFFAOYSA-N	>40
	RBZAGLIUHTVMFL-UHFFFAOYSA-N	>40
	HSJXOMZEPTVVQC-UHFFFAOYSA-N	>40
	PRAORRBPQXAGQD-UHFFFAOYSA-N	>40
	BMXOLQCTPIQVOD-UHFFFAOYSA-N	>40
	GYJACFGQPFXKCA-UHFFFAOYSA-N	>40
	PCRFOVGMSDFVLC-UHFFFAOYSA-N	>40
	FHXDSQYFCFWKAW-UHFFFAOYSA-N	>40
	OPTDAYWBFJRIGB-UHFFFAOYSA-N	>40
	GCUCIFQCGJIRNT-UHFFFAOYSA-N	>40

**Figure 2 – figure supplement 2.**

**PDXP inhibitor hits.**

Determination of half-maximal inhibitory constants (IC<sub>50</sub>) of 11 PDXP inhibitory compounds (see InChI Key for chemical substance identification) using purified murine PDXP and pyridoxal 5'-phosphate (PLP) as a substrate. Data marked with an asterisk (\*) are results of *n*=3 independent experiments. Because of the limited quantity of most compounds available for these assays, all other data are results of *n*=1 determinations. 7,8-DHF, 7,8-dihydroxyflavone; ~, approximate IC<sub>50</sub> value. **Source data** are available for this Table.



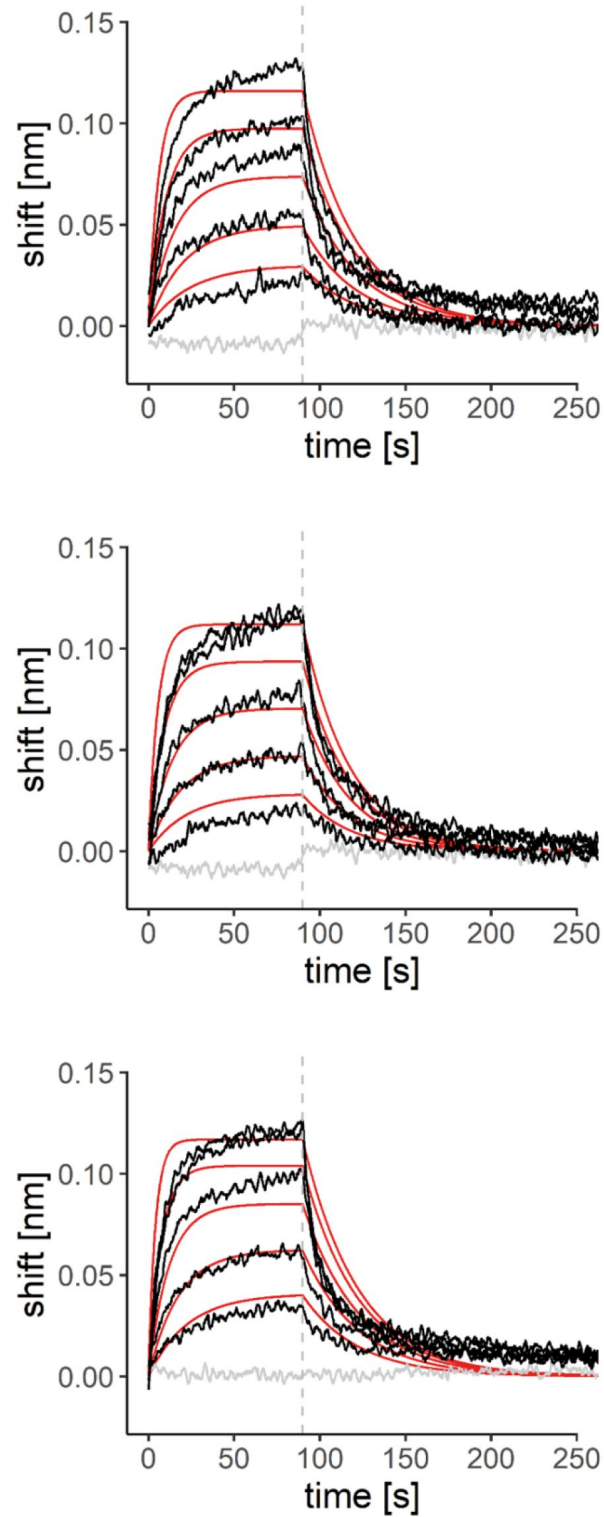


**Figure 2 – figure supplement 3.**

**BLI measurements of the interaction of 7,8-DHF with purified murine PDXP.**

Sensorgrams of three additional experiments overlaid with the global 1:1 binding model (red) and the negative control (gray). The dashed line indicates the start of the dissociation phase. **Source data** are available for this Figure.

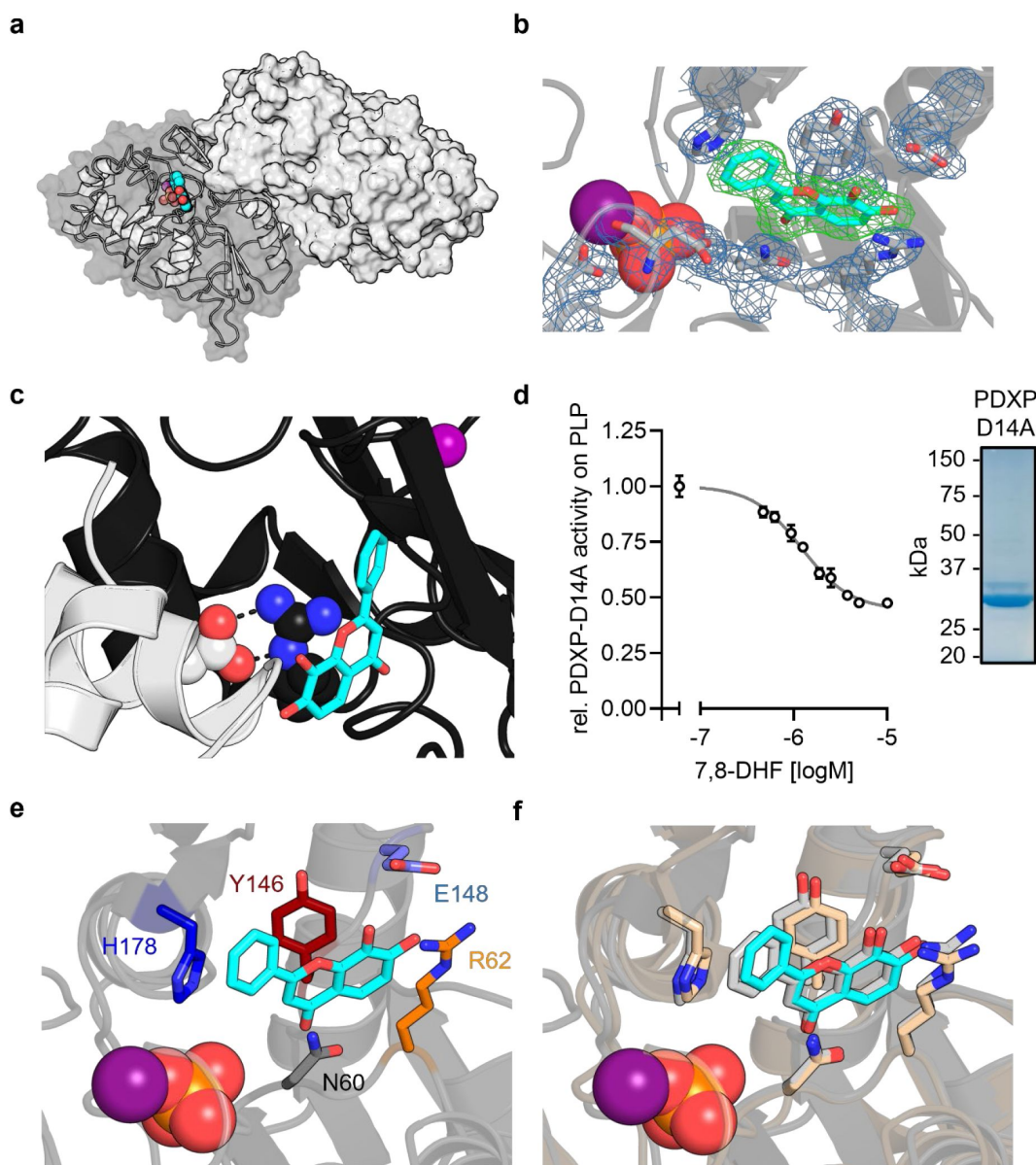


**Figure 3 – figure supplement 1.**

### X-ray crystal structures of murine PDXP in complex with 7,8-DHF.

(a) X-ray crystal structure of the assembled homodimeric, full-length murine PDXP in gray cartoon (protomer A) and surface (protomer B) representation. The model was refined to a resolution of 2.0 Å (PDB code 8QFW). 7,8-DHF is shown in sphere representation with its C-atoms in cyan. The  $Mg^{2+}$  ion is shown as deep purple sphere. The phosphate ion is shown as spheres with the phosphorous atom in orange. (b) The  $2F_o - F_c$  electron density map of the depicted amino acids is contoured at an RMSD of 1.0 in blue mesh and superimposed with the refined model. The  $F_o - F_c$  polder electron density map of 7,8-DHF is contoured at an RMSD of 3.0 in green mesh. (c) A salt bridge between Arg62 in the B-protomer (in black) and Asp14 of a symmetry-related A-protomer (in gray) blocks the 7,8-DHF binding site in the crystal lattice of murine PDXP. 7,8-DHF (in stick representation with cyan C-atoms) is modeled based on the A-protomer. (d) In vitro phosphatase activity of the purified PDXP-D14A variant in the presence of 7,8-DHF. Data are mean values  $\pm$  S.D. of  $n=3$  independent experiments. Apparently missing error bars are hidden by the symbols. The purity of PDXP-D14A is shown in the Coomassie Blue-stained gel on the right. (e) Structural details of bound 7,8-DHF and adjacent residues of the active site of mPDXP (in gray cartoon representation). (f) Superimposition of the 7,8-DHF binding sites in the phosphate-containing murine PDXP (shown in gray) and human PDXP (in wheat yellow) structures. The corresponding amino acids are shown as gray or wheat yellow-colored sticks. 7,8-DHF bound to murine or human PDXP is shown as sticks colored in gray or cyan, respectively. The position of the  $Mg^{2+}$  and phosphate ions is based on human PDXP. **Source data** are available for this Figure.

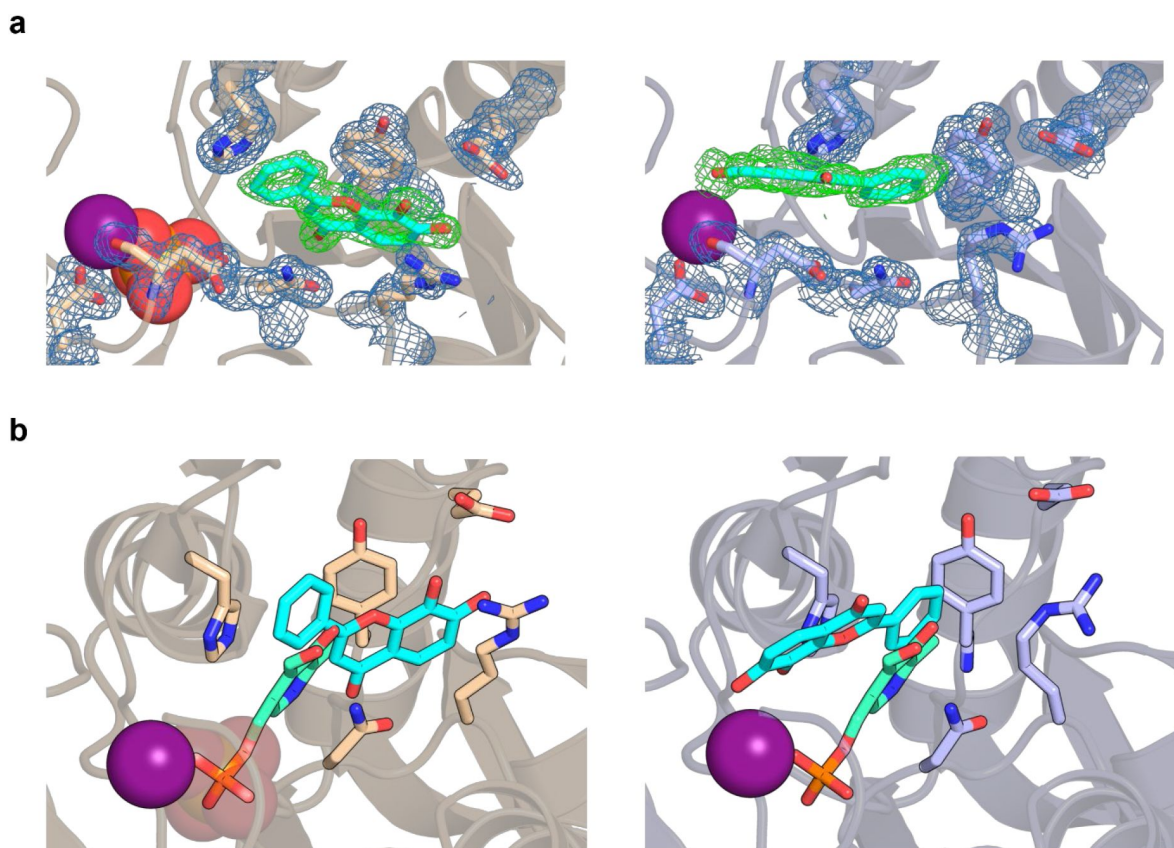


**Figure 3 - figure supplement 2.**

### 7,8-DHF coordination in PDXP.

(a) The  $2F_o - F_c$  electron density map of the depicted amino acids is contoured at an RMSD of 1.0 in blue mesh and superimposed with the refined model. The  $F_o - F_c$  polder electron density map of 7,8-DHF is contoured at an RMSD of 3.0 in green mesh. The  $Mg^{2+}$  ion is shown as a deep purple sphere. The phosphate ion is shown as a sphere with the phosphorous atom in orange. *Left panel*, human PDXP with phosphate (cartoon representation in wheat yellow); *right panel*, human PDXP without phosphate (cartoon representation in light blue). (b) Comparison of the 7,8-DHF and PLP binding sites in human PDXP with phosphate (wheat yellow, *left panel*), or human PDXP without phosphate (light blue, *right panel*). 7,8-DHF is shown in stick representation with cyan C-atoms. PLP (in stick representation with green C-atoms) was modelled based on a superposition of the human PDXP-PLP complex (PDB code 2CFT).

```

PDXP_HUMAN   MARCERLRGAALRDVLGRAQGVLFDCDGVLWNGERAVPGAPELLERLARAGKAALFVSN 60
PDXP_MOUSE   MARCERLRGAALRDVLGQAQGVLFDCDGVLWNGERIVPGAPELLQLRARAGKNTLFVSN 60
*****:***** *****:***** :*****

PDXP_HUMAN   SRRARPELALRFARLGFGLRAEQLFSSALCAARLLRQLPGPPDAPGAVFVLGGEG LRA 120
PDXP_MOUSE   SRRARPELALRFARLGFAGLRAEQLFSSALCAARLLRQLSGPPDASGAVFVLGGEG LRA 120
*****.***** ***** *****

PDXP_HUMAN   ELRAAGLRLAGDPSAGDGAAPRVRAVLVGYDEHFSFAKLREACAHLRDPECLLVATDRDP 180
PDXP_MOUSE   ELRAAGLRLAGDP---GEDPRVRAVLVGYDEQFSFRLTEACAHLRDPDCLLVATDRDP 176
***** * *****:***: * *****:*****

PDXP_HUMAN   WHPLSDGSRTPGTGLAAAVETASGRQALVVGKPSPYMFECITENFSIDPARTLMVGDRL 240
PDXP_MOUSE   WHPLSDGSRTPGTGLAAAVETASGRQALVVGKPSPYMFQCITEDFSVDPARTLMVGDRL 236
*****:***:*.*****

PDXP_HUMAN   ETDILFGHRCGMTTTLTGTGVSRL EEAQAYLAAGQHDLVPHYVYESIADLTEGLE D 296
PDXP_MOUSE   ETDILFGHRCGMTTTLTGTGVSRL EEAQAYLTAGQRDLVPHYVYESIADLMEGLE D 292
*****:***:***** *****

```

**Figure 3 – figure supplement 3.**

**Alignment of human and murine PDXP.**

Protein sequences of human PDXP (UniProtKB Q96GD0) and murine PDXP (UniProtKB P60487) were aligned with the EMBL-EBI multiple sequence alignment tool Clustal Omega version 1.2.4. PDXP residues found to engage in 7,8-DHF interactions (highlighted in red color) are identical in human and murine PDXP.

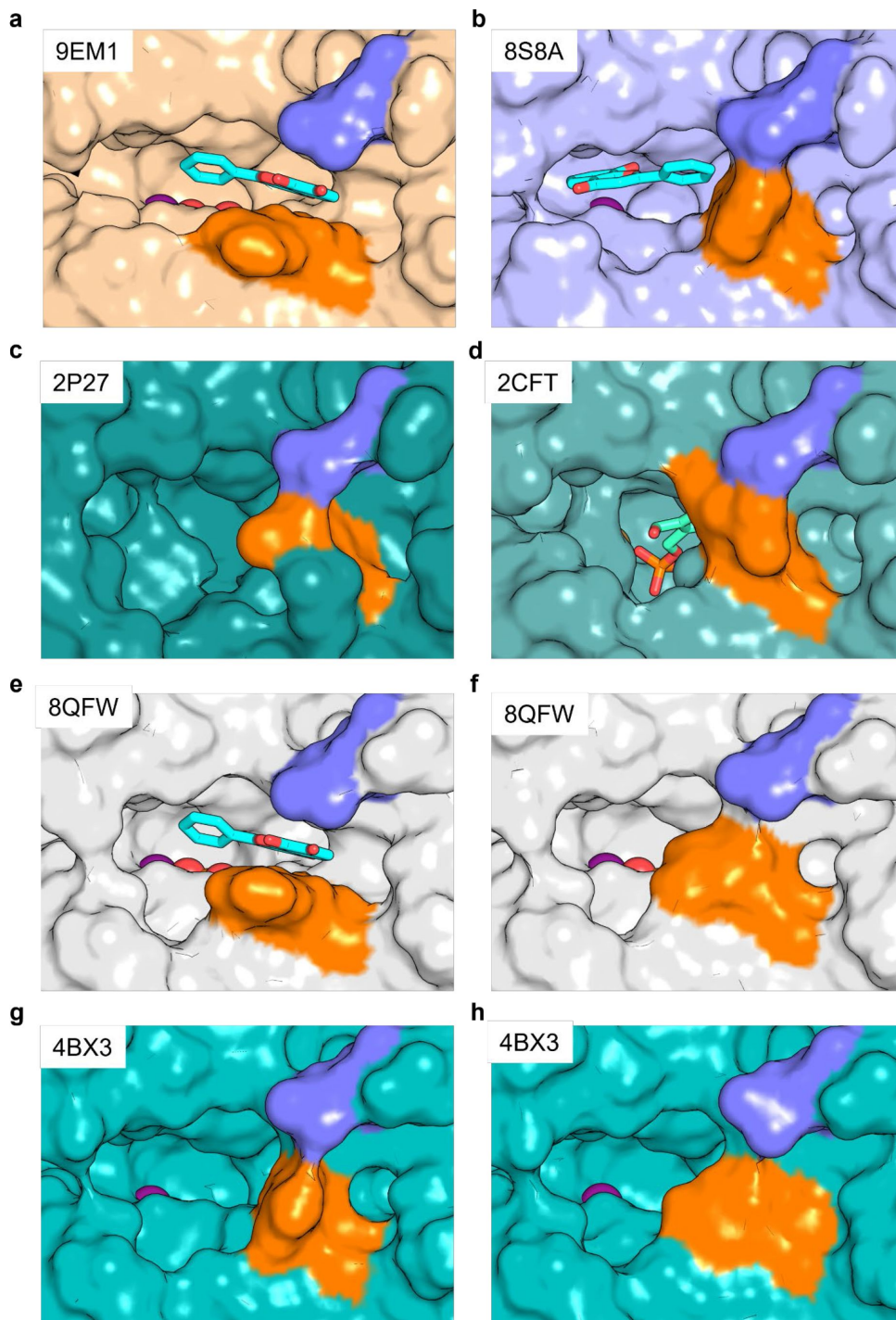


**Figure 3 - figure supplement 4.**

**Salt bridge formation between Glu152 (Glu148) and Arg62 gates the active site entrance in PDXP.**

Shown are views of the active site entrance in (a) hPDXP + 7,8-DHF with  $\text{PO}_4^{3-}$ , (b) hPDXP + 7,8-DHF without  $\text{PO}_4^{3-}$ , (c) apo-hPDXP, (d) hPDXP + PLP, (e) mPDXP + 7,8-DHF with  $\text{PO}_4^{3-}$ , chain A, (f) mPDXP + 7,8-DHF with  $\text{PO}_4^{3-}$ , chain B (inhibitor-free), (g) apo-mPDXP, chain A, (h) apo-mPDXP, chain B. The cap domain residue Glu152 in hPDXP (corresponding to Glu148 in mPDXP) is shown in blue, and the core domain residue Arg62 in hPDXP and mPDXP is shown in orange. 7,8-DHF is shown in stick representation with C-atoms in cyan. PLP is shown in stick representation with C-atoms in light green. The phosphate is shown in sphere representation with the phosphorous atom in orange.  $\text{Mg}^{2+}$  is shown as a deep purple sphere. hPDXP, human PDXP; mPDXP, murine PDXP. The respective PDB entries are indicated.

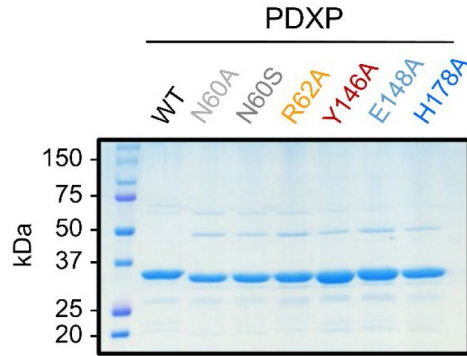


**Figure 3 – figure supplement 5.**

**Purity of the employed PDXP and PDXP variants.**

A Coomassie Blue-stained gel is shown.

## References

1. Bowling F. G. (2011) **Pyridoxine supply in human development** *Semin Cell Dev Biol* **22**:611–618
2. Wilson M. P., Plecko B., Mills P. B., Clayton P. T. (2019) **Disorders affecting vitamin B(6) metabolism** *J Inherit Metab Dis* **42**:629–646
3. di Salvo M. L., Safo M. K., Contestabile R. (2012) **Biomedical aspects of pyridoxal 5'-phosphate availability** *Front Biosci (Elite Ed)* **4**:897–913
4. Mitchell E. S., Conus N., Kaput J. (2014) **B vitamin polymorphisms and behavior: evidence of associations with neurodevelopment, depression, schizophrenia, bipolar disorder and cognitive decline** *Neurosci Biobehav Rev* **47**:307–320
5. Malouf R., Grimley Evans J. (2003) **The effect of vitamin B6 on cognition** *Cochrane Database Syst Rev* <https://doi.org/10.1002/14651858.CD004393>
6. Hughes C. F., et al. (2017) **B-Vitamin Intake and Biomarker Status in Relation to Cognitive Decline in Healthy Older Adults in a 4-Year Follow-Up Study** *Nutrients* **9**
7. Jannusch K., et al. (2017) **A Complex Interplay of Vitamin B1 and B6 Metabolism with Cognition, Brain Structure, and Functional Connectivity in Older Adults** *Front Neurosci* **11**
8. Xu H., Wang S., Gao F., Li C. (2022) **Vitamin B(6), B(9), and B(12) Intakes and Cognitive Performance in Elders: National Health and Nutrition Examination Survey, 2011-2014** *Neuropsychiatr Dis Treat* **18**:537–553
9. Elias M. F., et al. (2006) **Homocysteine, folate, and vitamins B6 and B12 blood levels in relation to cognitive performance: the Maine-Syracuse study** *Psychosom Med* **68**:547–554
10. Tomioka Y., et al. (2018) **Decreased serum pyridoxal levels in schizophrenia: meta-analysis and Mendelian randomization analysis** *J Psychiatry Neurosci* **43**:194–200
11. Toriumi K., et al. (2021) **Vitamin B6 deficiency hyperactivates the noradrenergic system, leading to social deficits and cognitive impairment** *Transl Psychiatry* **11**
12. Arai M., et al. (2010) **Enhanced carbonyl stress in a subpopulation of schizophrenia** *Arch Gen Psychiatry* **67**:589–597
13. Paul B. D. (2021) **Neuroprotective Roles of the Reverse Transsulfuration Pathway in Alzheimer's Disease** *Front Aging Neurosci* **13**
14. Ueland P. M., McCann A., Midttun O., Ulvik A. (2017) **Inflammation, vitamin B6 and related pathways** *Mol Aspects Med* **53**:10–27
15. Danielski L. G., et al. (2018) **Vitamin B(6) Reduces Neurochemical and Long-Term Cognitive Alterations After Polymicrobial Sepsis: Involvement of the Kynurenine Pathway Modulation** *Mol Neurobiol* **55**:5255–5268
16. Wang Z., Zhu W., Xing Y., Jia J., Tang Y. (2022) **B vitamins and prevention of cognitive decline and incident dementia: a systematic review and meta-analysis** *Nutr Rev* **80**:931–949

17. Behrens A., Graessel E., Pendergrass A., Donath C. (2020) **Vitamin B-Can it prevent cognitive decline? A systematic review and meta-analysis** *Syst Rev* **9**
18. Hassel B., Rogne A. G., Hope S. (2019) **Intellectual Disability Associated With Pyridoxine-Responsive Epilepsies: The Need to Protect Cognitive Development** *Front Psychiatry* **10**
19. Rutjes A. W., et al. (2018) **Vitamin and mineral supplementation for maintaining cognitive function in cognitively healthy people in mid and late life** *Cochrane Database Syst Rev* **12**
20. Smith A. D., Refsum H. (2016) **Homocysteine, B Vitamins, and Cognitive Impairment** *Annu Rev Nutr* **36**:211–239
21. Aisen P. S., et al. (2008) **High-dose B vitamin supplementation and cognitive decline in Alzheimer disease: a randomized controlled trial** *JAMA* **300**:1774–1783
22. Douaud G., et al. (2013) **Preventing Alzheimer’s disease-related gray matter atrophy by B-vitamin treatment** *Proc Natl Acad Sci U S A* **110**:9523–9528
23. Percudani R., Peracchi A. (2003) **A genomic overview of pyridoxal-phosphate-dependent enzymes** *EMBO Rep* **4**:850–854
24. Eliot A. C., Kirsch J. F. (2004) **Pyridoxal phosphate enzymes: mechanistic, structural, and evolutionary considerations** *Annu Rev Biochem* **73**:383–415
25. Percudani R., Peracchi A. (2009) **The B6 database: a tool for the description and classification of vitamin B6-dependent enzymatic activities and of the corresponding protein families** *BMC Bioinformatics* **10**
26. Parra M., Stahl S., Hellmann H. (2018) **Vitamin B(6) and Its Role in Cell Metabolism and Physiology** *Cells* **7**
27. Ciapaite J., et al. (2023) **Maintenance of cellular vitamin B(6) levels and mitochondrial oxidative function depend on pyridoxal 5’-phosphate homeostasis protein (PLPHP)** *J Biol Chem* <https://doi.org/10.1016/j.jbc.2023.105047>
28. Fux A., Sieber S. A. (2020) **Biochemical and Proteomic Studies of Human Pyridoxal 5’-Phosphate-Binding Protein (PLPBP)** *ACS Chem Biol* **15**:254–261
29. Jang Y. M., et al. (2003) **Human pyridoxal phosphatase. Molecular cloning, functional expression, and tissue distribution** *J Biol Chem* **278**:50040–50046
30. Jeanclos E., et al. (2019) **Improved cognition, mild anxiety-like behavior and decreased motor performance in pyridoxal phosphatase-deficient mice** *Biochim Biophys Acta Mol Basis Dis* **1865**:193–205
31. Liu C., Chan C. B., Ye K. (2016) **7,8-dihydroxyflavone, a small molecular TrkB agonist, is useful for treating various BDNF-implicated human disorders** *Transl Neurodegener* **5**
32. Wang C. S., Kavalali E. T., Monteggia L. M. (2022) **BDNF signaling in context: From synaptic regulation to psychiatric disorders** *Cell* **185**:62–76
33. Boltaev U., et al. (2017) **Multiplex quantitative assays indicate a need for reevaluating reported small-molecule TrkB agonists** *Sci Signal* **10**



34. Pankiewicz P., et al. (2021) **Do Small Molecules Activate the TrkB Receptor in the Same Manner as BDNF? Limitations of Published TrkB Low Molecular Agonists and Screening for Novel TrkB Orthosteric Agonists** *Pharmaceuticals (Basel)* **14**
35. Todd D., et al. (2014) **A monoclonal antibody TrkB receptor agonist as a potential therapeutic for Huntington's disease** *PLoS One* **9**
36. Chen J., et al. (2011) **Antioxidant activity of 7,8-dihydroxyflavone provides neuroprotection against glutamate-induced toxicity** *Neurosci Lett* **499**:181–185
37. Fonda M. L., Eggers D. K., Auerbach S., Fritsch L. (1980) **Vitamin B-6 metabolism in the brains of young adult and senescent mice** *Exp Gerontol* **15**:473–479
38. Gohla A. (2019) **Do metabolic HAD phosphatases moonlight as protein phosphatases?** *Biochim Biophys Acta Mol Cell Res* **1866**:153–166
39. Seifried A., et al. (2014) **Evolutionary and structural analyses of mammalian haloacid dehalogenase-type phosphatases AUM and chronophin provide insight into the basis of their different substrate specificities** *J Biol Chem* **289**:3416–3431
40. Jeanclos E., et al. (2022) **Glycolytic flux control by drugging phosphoglycolate phosphatase** *Nat Commun* **13**
41. Congreve M., Carr R., Murray C., Jhoti H. (2003) **A 'rule of three' for fragment-based lead discovery?** *Drug Discov Today* **8**:876–877
42. O'Connell J., et al. (2019) **Small molecules that inhibit TNF signalling by stabilising an asymmetric form of the trimer** *Nat Commun* **10**
43. Seifried A., Schultz J., Gohla A. (2013) **Human HAD phosphatases: structure, mechanism, and roles in health and disease** *Febs j* **280**:549–571
44. Burroughs A. M., Allen K. N., Dunaway-Mariano D., Aravind L. (2006) **Evolutionary genomics of the HAD superfamily: understanding the structural adaptations and catalytic diversity in a superfamily of phosphoesterases and allied enzymes** *J Mol Biol* **361**:1003–1034
45. Huang H., et al. (2015) **Panoramic view of a superfamily of phosphatases through substrate profiling** *Proc Natl Acad Sci U S A* **112**:E1974–1983
46. Proenca C., et al. (2018) **Inhibition of protein tyrosine phosphatase 1B by flavonoids: A structure - activity relationship study** *Food Chem Toxicol* **111**:474–481
47. Bianchi V., Spychala J. (2003) **Mammalian 5'-nucleotidases** *J Biol Chem* **278**:46195–46198
48. Kestler C., et al. (2014) **Chronophin dimerization is required for proper positioning of its substrate specificity loop** *J Biol Chem* **289**:3094–3103
49. Knobloch G., et al. (2015) **Synthesis of hydrolysis-resistant pyridoxal 5'-phosphate analogs and their biochemical and X-ray crystallographic characterization with the pyridoxal phosphatase chronophin** *Bioorg Med Chem* **23**:2819–2827
50. Zhang Z., et al. (2014) **7,8-dihydroxyflavone prevents synaptic loss and memory deficits in a mouse model of Alzheimer's disease** *Neuropsychopharmacology* **39**:638–650

51. Devi L., Ohno M. (2012) **7,8-dihydroxyflavone, a small-molecule TrkB agonist, reverses memory deficits and BACE1 elevation in a mouse model of Alzheimer's disease** *Neuropsychopharmacology* **37**:434–444
52. Bollen E., et al. (2013) **7,8-Dihydroxyflavone improves memory consolidation processes in rats and mice** *Behav Brain Res* **257**:8–12
53. Castello N. A., et al. (2014) **7,8-Dihydroxyflavone, a small molecule TrkB agonist, improves spatial memory and increases thin spine density in a mouse model of Alzheimer disease-like neuronal loss** *PLoS One* **9**
54. Aytan N., et al. (2018) **Protective effects of 7,8-dihydroxyflavone on neuropathological and neurochemical changes in a mouse model of Alzheimer's disease** *Eur J Pharmacol* **828**:9–17
55. Gao L., et al. (2016) **TrkB activation by 7, 8-dihydroxyflavone increases synapse AMPA subunits and ameliorates spatial memory deficits in a mouse model of Alzheimer's disease** *J Neurochem* **136**:620–636
56. Akhtar A., Dhaliwal J., Sah S. P. (2021) **7,8-Dihydroxyflavone improves cognitive functions in ICV-STZ rat model of sporadic Alzheimer's disease by reversing oxidative stress, mitochondrial dysfunction, and insulin resistance** *Psychopharmacology (Berl)* **238**:1991–2009
57. Hsiao Y. H., Hung H. C., Chen S. H., Gean P. W. (2014) **Social interaction rescues memory deficit in an animal model of Alzheimer's disease by increasing BDNF-dependent hippocampal neurogenesis** *J Neurosci* **34**:16207–16219
58. Blugeot A., et al. (2011) **Vulnerability to depression: from brain neuroplasticity to identification of biomarkers** *J Neurosci* **31**:12889–12899
59. Zhang J. C., et al. (2014) **Antidepressant effects of TrkB ligands on depression-like behavior and dendritic changes in mice after inflammation** *Int J Neuropsychopharmacol* **18**
60. Yao W., et al. (2016) **Role of Keap1-Nrf2 signaling in depression and dietary intake of glucoraphanin confers stress resilience in mice** *Sci Rep* **6**
61. Zhang M. W., Zhang S. F., Li Z. H., Han F. (2016) **7,8-Dihydroxyflavone reverses the depressive symptoms in mouse chronic mild stress** *Neurosci Lett* **635**:33–38
62. Li Y., et al. (2022) **Inflammation-activated C/EBPbeta mediates high-fat diet-induced depression-like behaviors in mice** *Front Mol Neurosci* **15**
63. Amin N., et al. (2020) **Optimized integration of fluoxetine and 7, 8-dihydroxyflavone as an efficient therapy for reversing depressive-like behavior in mice during the perimenopausal period** *Prog Neuropsychopharmacol Biol Psychiatry* **101**
64. Jaehne E. J., et al. (2021) **TrkB agonist 7,8-dihydroxyflavone reverses an induced prepulse inhibition deficit selectively in maternal immune activation offspring: implications for schizophrenia** *Behav Pharmacol* **32**:404–412
65. Han M., et al. (2016) **Intake of 7,8-Dihydroxyflavone During Juvenile and Adolescent Stages Prevents Onset of Psychosis in Adult Offspring After Maternal Immune Activation** *Sci Rep* **6**

66. Yang Y. J., et al. (2014) **Small-molecule TrkB agonist 7,8-dihydroxyflavone reverses cognitive and synaptic plasticity deficits in a rat model of schizophrenia** *Pharmacol Biochem Behav* **122**:30–36
67. Han M., Zhang J. C., Hashimoto K. (2017) **Increased Levels of C1q in the Prefrontal Cortex of Adult Offspring after Maternal Immune Activation: Prevention by 7,8-Dihydroxyflavone** *Clin Psychopharmacol Neurosci* **15**:64–67
68. Ren Q., et al. (2013) **Effects of TrkB agonist 7,8-dihydroxyflavone on sensory gating deficits in mice after administration of methamphetamine** *Pharmacol Biochem Behav* **106**:124–127
69. Becker C., et al. (2015) **Predicting and treating stress-induced vulnerability to epilepsy and depression** *Ann Neurol* **78**:128–136
70. Guarino A., et al. (2022) **Low-dose 7,8-Dihydroxyflavone Administration After Status Epilepticus Prevents Epilepsy Development** *Neurotherapeutics* **19**:1951–1965
71. Johnson R. A., et al. (2012) **7,8-dihydroxyflavone exhibits therapeutic efficacy in a mouse model of Rett syndrome** *J Appl Physiol(1985)* **112**:704–710
72. Kang M. S., et al. (2017) **Autism-like behavior caused by deletion of vaccinia-related kinase 3 is improved by TrkB stimulation** *J Exp Med* **214**:2947–2966
73. Lee Y., Han P. L. (2019) **Early-Life Stress in D2 Heterozygous Mice Promotes Autistic-like Behaviors through the Downregulation of the BDNF-TrkB Pathway in the Dorsal Striatum** *Exp Neurol* **28**:337–351
74. Chen Y. S., et al. (2023) **Early 7,8-Dihydroxyflavone Administration Ameliorates Synaptic and Behavioral Deficits in the Young FXS Animal Model by Acting on BDNF-TrkB Pathway** *Mol Neurobiol* **60**:2539–2552
75. Majewski M., Kozłowska A., Thoene M., Lepiarczyk E., Grzegorzewski W. J. (2016) **Overview of the role of vitamins and minerals on the kynurenine pathway in health and disease** *J Physiol Pharmacol* **67**:3–19
76. Sorolla M. A., et al. (2016) **Impaired PLP-dependent metabolism in brain samples from Huntington disease patients and transgenic R6/1 mice** *Metab Brain Dis* **31**:579–586
77. Jang S. W., et al. (2010) **A selective TrkB agonist with potent neurotrophic activities by 7,8-dihydroxyflavone** *Proc Natl Acad Sci U S A* **107**:2687–2692
78. Kobayashi K., Suzuki H. (2018) **Synapse-selective rapid potentiation of hippocampal synaptic transmission by 7,8-dihydroxyflavone** *Neuropsychopharmacol Rep* **38**:197–203
79. Talwar D., et al. (2003) **Optimisation and validation of a sensitive high-performance liquid chromatography assay for routine measurement of pyridoxal 5-phosphate in human plasma and red cells using pre-column semicarbazide derivatisation** *Journal of chromatography. B, Analytical technologies in the biomedical and life sciences* **792**:333–343
80. Studier F. W. (2005) **Protein production by auto-induction in high density shaking cultures** *Protein Expr Purif* **41**:207–234
81. Wartchow C. A., et al. (2011) **Biosensor-based small molecule fragment screening with biolayer interferometry** *J Comput Aided Mol Des* **25**:669–676

82. Kabsch W. (2010) **Xds**. *Acta crystallographica Section D, Biological crystallography* **66**:125–132
83. Evans P. R., Murshudov G. N. (2013) **How good are my data and what is the resolution?** *Acta crystallographica. Section D, Biological crystallography* **69**:1204–1214
84. Winn M. D., et al. (2011) **Overview of the CCP4 suite and current developments** *Acta crystallographica. Section D, Biological crystallography* **67**:235–242
85. McCoy A. J., et al. (2007) **Phaser crystallographic software** *J Appl Crystallogr* **40**:658–674
86. Adams P. D., et al. (2010) **PHENIX: a comprehensive Python-based system for macromolecular structure solution** *Acta crystallographica. Section D, Biological crystallography* **66**:213–221
87. Emsley P., Lohkamp B., Scott W. G., Cowtan K. (2010) **Features and development of Coot** *Acta crystallographica. Section D, Biological crystallography* **66**:486–501
88. Schrodinger LLC (2021) **The PyMOL Molecular Graphics System, Version 2.5.1**

## Article and author information

### Marian Brenner

Institute of Pharmacology and Toxicology, University of Würzburg, Germany  
ORCID iD: [0009-0001-3781-1056](https://orcid.org/0009-0001-3781-1056)

### Christoph Zink

Institute of Pharmacology and Toxicology, University of Würzburg, Germany

### Linda Witzinger

Institute of Pharmacology and Toxicology, University of Würzburg, Germany

### Angelika Keller

Institute of Pharmacology and Toxicology, University of Würzburg, Germany

### Kerstin Hadamek

Institute of Pharmacology and Toxicology, University of Würzburg, Germany

### Sebastian Bothe

Rudolf Virchow Center for Integrative and Translational Bioimaging, University of Würzburg, Germany  
ORCID iD: [0000-0001-6408-6112](https://orcid.org/0000-0001-6408-6112)

### Martin Neuenschwander

Leibniz-Forschungsinstitut für Molekulare Pharmakologie-FMP, Berlin, Germany

### Carmen Villmann

Institute of Clinical Neurobiology, University Hospital, University of Würzburg, Germany  
ORCID iD: [0000-0003-1498-6950](https://orcid.org/0000-0003-1498-6950)

### Jens Peter von Kries

Leibniz-Forschungsinstitut für Molekulare Pharmakologie-FMP, Berlin, Germany

**Hermann Schindelin**

Rudolf Virchow Center for Integrative and Translational Bioimaging, University of Würzburg, Germany

ORCID iD: [0000-0002-2067-3187](https://orcid.org/0000-0002-2067-3187)

**Elisabeth Jeanclos**

Institute of Pharmacology and Toxicology, University of Würzburg, Germany

**For correspondence:** [elisabeth.jeanclos@uni-wuerzburg.de](mailto:elisabeth.jeanclos@uni-wuerzburg.de)

**Antje Gohla**

Institute of Pharmacology and Toxicology, University of Würzburg, Germany

**For correspondence:** [antje.gohla@uni-wuerzburg.de](mailto:antje.gohla@uni-wuerzburg.de)

ORCID iD: [0000-0002-7442-1487](https://orcid.org/0000-0002-7442-1487)

**Copyright**

© 2024, Brenner et al.

This article is distributed under the terms of the [Creative Commons Attribution License](https://creativecommons.org/licenses/by/4.0/), which permits unrestricted use and redistribution provided that the original author and source are credited.

**Editors**

Reviewing Editor

**Moses Chao**

New York University Langone Medical Center, New York, United States of America

Senior Editor

**David Ron**

University of Cambridge, Cambridge, United Kingdom

**Reviewer #1 (Public Review):**

Summary:

This manuscript set out to identify selective inhibitors of the pyridoxal phosphatase (PDXP). Previous studies had demonstrated improvements in cognition upon removal of PDXP, and here the authors reveal that this correlates with an increase in pyridoxal phosphate (PLP; PDXP substrate and an active coenzyme form of vitamin B6) with age. Since several pathologies are associated with decreased vitamin B6, the authors propose that PDXP is an attractive therapeutic target in the prevention/treatment of cognitive decline. Following high throughput and secondary small molecule screens, they identify two selective inhibitors. They follow up on 7, 8 dihydroxyflavone (DHF). Following structure-activity relationship and selectivity studies, the authors then solve a co-crystal structure of 7,8 DHF bound to the active site of PDXP, supporting a competitive mode of PDXP inhibition. Finally, they find that treating hippocampal neurons with 7,8 DHF increases PLP levels in a WT but not PDXP KO context. The authors note that 7,8 DHF has been used in numerous rodent neuropathology models to improve outcomes. 7, 8 DHF activity was previously attributed to activation of the receptor tyrosine kinase TrkB, although this appears to be controversial. The present study raises the possibility that it instead/also acts through modulation of PLP levels via PDXP, and is an important area for future work.

**Strengths:**

The strengths of the work are in the comprehensive, thorough, and unbiased nature of the analyses revealing the potential for therapeutic intervention in a number of pathologies.

**Weaknesses:**

Potential weaknesses include the poor solubility of 7,8 DHF that might limit its bioavailability given its relatively low potency (IC<sub>50</sub>= 0.8 μM), which was not improved by SAR. The solubility issues of 7,8 DHF have been discussed at length in the authors' response to Reviewer #3. In particular, the solubility of 7,8 DHF has been found to be variable due to the concentration and buffer conditions. The 7,8 DHF compound has an extended residence time and the co-crystal structure could aid the design of more potent molecules and would be of interest to those in the pharmaceutical industry. The images related to crystal structure have been improved with additional structural analysis of PDXP in a complex of 7,8-DHF (see revised Figure 3).

<https://doi.org/10.7554/eLife.93094.2.sa2>

**Reviewer #2 (Public Review):****Summary:**

In this study, the authors performed a screening for PDXP inhibitors to identify compounds that could increase levels of pyridoxal 5'- phosphate (PLP), the co-enzymatically active form of vitamin B6. For the screening of inhibitors, they first evaluated a library of about 42,000 compounds for activators and inhibitors of PDXP and secondly, they validated the inhibitor compounds with a counter-screening against PGP, a close PDXP relative. The final narrowing down to 7,8-DHF was done using PLP as a substrate and confirmed the efficacy of this flavonoid as an inhibitor of PDXP function. Physiologically, the authors show that, by acutely treating isolated wild-type hippocampal neurons with 7,8-DHF they could detect an increase in the ratio of PLP/PL compared to control cultures. This effect was not seen in PDXP KO neurons.

**Strengths:**

The screening and validation of the PDXP inhibitors have been done very well because the authors have performed crystallographic analysis, a counter screening, and mutation analysis. This is very important because such rigor has not been applied to the original report of 7,8 DHF as an agonist for TrkB. Which is why there is so much controversy on this finding.

**Weaknesses:**

As mentioned in the summary report the study may benefit from some in vivo analysis of PLP levels following 7,8-DHF treatment, although I acknowledge that it may be challenging because of the working out of the dosage and timing of the procedure.

<https://doi.org/10.7554/eLife.93094.2.sa1>

**Reviewer #3 (Public Review):**

This is interesting biology. Vitamin B6 deficiency has been linked to cognitive impairment. It is not clear whether supplements are effective in restoring functional B6 levels. Vitamin B6 is composed of pyridoxal compounds and their phosphorylated forms, with pyridoxal 5-phosphate (PLP) being of particular importance. The levels of PLP are determined by the

balance between pyridoxal kinase and phosphatase activities. The authors are testing the hypothesis that inhibition of pyridoxal phosphatase (PDXP) would arrest the age-dependent decline in PLP, offering an alternative therapeutic strategy to supplements. Published data illustrating that ablation of the Pdxp gene in mice led to increases in PLP levels and improvement in learning and memory trials are consistent with this hypothesis.

In this report, the authors conduct a screen of a library of ~40k small molecules and identify 7,8-dihydroxyflavone (DHF) as a candidate PDXP inhibitor. They present an initial characterization of this micromolar inhibitor, including a co-crystal structure of PDXP and 7,8-DHF. In addition, they demonstrate that treatment of cells with 7,8 DHP increases PLP levels. Overall, this study provides further validation of PDXP as a therapeutic target for the treatment of disorders associated with vitamin B6 deficiency and provides proof-of-concept for inhibition of the target with small-molecule drug candidates.

Strengths include the biological context, the focus on an interesting and under-studied class of protein phosphatases that includes several potential therapeutic targets, and the identification of a small molecule inhibitor that provides proof-of-concept for a new therapeutic strategy. Overall, the study has the potential to be an important development for the phosphatase field in general.

Weaknesses include the fact that the compound is very much an early-stage screening hit. It is an inhibitor with micromolar potency for which mechanisms of action other than inhibition of PDXP have been reported. Extensive further development will be required to demonstrate convincingly the extent to which its effects in cells are due to on-target inhibition of PDXP.

<https://doi.org/10.7554/eLife.93094.2.sa0>

#### **Author response:**

The following is the authors' response to the original reviews.

##### **eLife assessment**

*Following small molecule screens, this study provides convincing evidence that 7,8 dihydroxyflavone (DHF) is a competitive inhibitor of pyridoxal phosphatase. These results are important since they offer an alternative mechanism for the effects of 7,8 dihydroxyflavone in cognitive improvement in several mouse models. This paper is also significant due to the interest in the protein phosphatases and neurodegeneration fields.*

##### **Public Reviews:**

###### **Reviewer #1 (Public Review):**

*Summary:*

*Zink et al set out to identify selective inhibitors of the pyridoxal phosphatase (PDXP). Previous studies had demonstrated improvements in cognition upon removal of PDXP, and here the authors reveal that this correlates with an increase in pyridoxal phosphate (PLP; PDXP substrate and an active coenzyme form of vitamin B6) with age. Since several pathologies are associated with decreased vitamin B6, the authors propose that PDXP is an attractive therapeutic target in the prevention/treatment of cognitive decline. Following high throughput and secondary small molecule screens, they identify two selective inhibitors. They follow up on 7, 8 dihydroxyflavone (DHF). Following structure-activity relationship and selectivity studies, the authors then solve a co-crystal structure of 7,8 DHF bound to the active site of PDXP, supporting a competitive mode of PDXP*

*inhibition. Finally, they find that treating hippocampal neurons with 7,8 DHF increases PLP levels in a WT but not PDXP KO context. The authors note that 7,8 DHF has been used in numerous rodent neuropathology models to improve outcomes. 7, 8 DHF activity was previously attributed to activation of the receptor tyrosine kinase TrkB, although this appears to be controversial. The present study raises the possibility that it instead/also acts through modulation of PLP levels via PDXP, and is an important area for future work.*

**Strengths:**

*The strengths of the work are in the comprehensive, thorough, and unbiased nature of the analyses revealing the potential for therapeutic intervention in a number of pathologies.*

**Weaknesses:**

*Potential weaknesses include the poor solubility of 7,8 DHF that might limit its bioavailability given its relatively low potency ( $IC_{50} = 0.8 \mu M$ ), which was not improved by SAR. However, the compound has an extended residence time and the co-crystal structure could aid the design of more potent molecules and would be of interest to those in the pharmaceutical industry. The images related to crystal structure could be improved.*

**Reviewer #2 (Public Review):**

**Summary:**

*In this study, the authors performed a screening for PDXP inhibitors to identify compounds that could increase levels of pyridoxal 5'-phosphate (PLP), the co-enzymatically active form of vitamin B6. For the screening of inhibitors, they first evaluated a library of about 42,000 compounds for activators and inhibitors of PDXP and secondly, they validated the inhibitor compounds with a counter-screening against PGP, a close PDXP relative. The final narrowing down to 7,8-DHF was done using PLP as a substrate and confirmed the efficacy of this flavonoid as an inhibitor of PDXP function. Physiologically, the authors show that, by acutely treating isolated wild-type hippocampal neurons with 7,8-DHF they could detect an increase in the ratio of PLP/PL compared to control cultures. This effect was not seen in PDXP KO neurons.*

**Strengths:**

*The screening and validation of the PDXP inhibitors have been done very well because the authors have performed crystallographic analysis, a counter screening, and mutation analysis. This is very important because such rigor has not been applied to the original report of 7,8 DHF as an agonist for TrkB. Which is why there is so much controversy on this finding.*

**Weaknesses:**

*As mentioned in the summary report the study may benefit from some in vivo analysis of PLP levels following 7,8-DHF treatment, although I acknowledge that it may be challenging because of the working out of the dosage and timing of the procedure.*

**Reviewer #3 (Public Review):**

*This is interesting biology. Vitamin B6 deficiency has been linked to cognitive impairment. It is not clear whether supplements are effective in restoring functional B6 levels. Vitamin B6 is composed of pyridoxal compounds and their phosphorylated forms, with pyridoxal 5-phosphate (PLP) being of particular importance. The levels of PLP are determined by the balance between pyridoxal kinase and phosphatase activities. The authors are testing*



*the hypothesis that inhibition of pyridoxal phosphatase (PDXP) would arrest the age-dependent decline in PLP, offering an alternative therapeutic strategy to supplements. Published data illustrating that ablation of the Pdxp gene in mice led to increases in PLP levels and improvement in learning and memory trials are consistent with this hypothesis.*

*In this report, the authors conduct a screen of a library of ~40k small molecules and identify 7,8-dihydroxyflavone (DHF) as a candidate PDXP inhibitor. They present an initial characterization of this micromolar inhibitor, including a co-crystal structure of PDXP and 7,8-DHF. In addition, they demonstrate that treatment of cells with 7,8 DHP increases PLP levels. Overall, this study provides further validation of PDXP as a therapeutic target for the treatment of disorders associated with vitamin B6 deficiency and provides proof-of-concept for inhibition of the target with small-molecule drug candidates.*

*Strengths include the biological context, the focus on an interesting and under-studied class of protein phosphatases that includes several potential therapeutic targets, and the identification of a small molecule inhibitor that provides proof-of-concept for a new therapeutic strategy. Overall, the study has the potential to be an important development for the phosphatase field in general.*

*Weaknesses include the fact that the compound is very much an early-stage screening hit. It is an inhibitor with micromolar potency for which mechanisms of action other than inhibition of PDXP have been reported. Extensive further development will be required to demonstrate convincingly the extent to which its effects in cells are due to on-target inhibition of PDXP.*

**Recommendations for the authors:**

*There is general agreement that the study represents an advance regarding the mechanisms of pyridoxal phosphatase and 7,8 DHF. From the reviewers' comments, several major questions and considerations are raised, followed by their detailed remarks:*

*(1) More analysis of the solubility and dose of 7,8 DHF with regard to the 50% inhibition and the salt bridge of the B protomer, as raised by the reviewers.*

*(2) Is there a possible involvement of another phosphatase?*

*(3) Does 7,8 DHF cause an effect upon TrkB tyrosine phosphorylation?*

We thank the Reviewers and Editors for their fair and constructive comments and suggestions. We have performed additional experiments to address these questions and considerations. In addition, we have generated two new high-resolving (1.5 Å) crystal structures of human PDXP in complex with 7,8-DHF that substantially expand our understanding of 7,8-DHF-mediated PDXP inhibition. The scientist who performed this work for the revision of our manuscript has been added as an author (shared first authorship).

We believe that the insights gained from these new data have further strengthened and improved the quality of our manuscript. Together, our data provide compelling evidence that 7,8-dihydroxyflavone is a direct and competitive inhibitor of pyridoxal phosphatase.

Please find our point-by-point responses to the Public Reviews that are not addressed in the Recommendations for the Authors, and the Recommendations for the Authors below.

**Reviewer #2:**

*As mentioned in the summary report the study may benefit from some in vivo analysis of PLP levels following 7,8-DHF treatment, although I acknowledge that it may be challenging because of the working out of the dosage and timing of the procedure.*

We agree that an in vivo analysis of PLP levels following 7,8-DHF treatment could be informative for the further evaluation of a possible mechanistic link between the reported effects of this compound and PDXP/vitamin B6. However, we currently do not have a corresponding animal experimentation permission in place and are unlikely to obtain such a permit within a reasonable time frame for this revision.

**Recommendations For The Authors:**

**Reviewer #1:**

*The work is already well-written, comprehensive, and convincing.*

*Suggestions that could improve the manuscript.*

*(1) Include a protein tyrosine phosphatase (PTP) in the selectivity analysis. One possibility is that 7,8 DHF acts on a PTP (such as PTP1B), leading to TrkB activation by preventing dephosphorylation. I note that a previous study has looked at SAR for flavones with PTP1B (PMID: 29175190), which is worth discussion.*

We thank the reviewer for bringing this interesting possibility to our attention. We were not aware of the SAR study for flavonoids with PTP1B by Proenca et al. but have now tested the effect of 7,8-DHF on PTP1B, referring to this paper. As shown in Figure 2d, PTP1B was not inhibited by 7,8-DHF at a concentration of 5 or 10  $\mu$ M. At the highest tested concentration of 40  $\mu$ M, 7,8-DHF inhibited PTP1B merely by  $\sim$ 20%. For comparison, compound C13 (3-hydroxy-7,8-dihydroxybenzylflavone-3',4'-dihydroxymethyl-phenyl), which emerged as the most active flavonoid in the SAR study by Proenca et al. inhibited PTP1B with an IC<sub>50</sub> of 10  $\mu$ M. Consistent with the results of these authors, our finding confirms that less polar substituents, such as O-benzyl groups at positions 7 and 8, and O-methyl groups at positions 3' and 4' of the flavone scaffold, are important for the ability of flavonoids to effectively inhibit PTP1B. We conclude that PTP1B inhibition by 7,8-DHF is unlikely to be a primary contributor to the reported cellular and in vivo effects of this flavone.

In addition to PTP1B, we have now additionally tested the effect of 7,8-DHF on the serine/threonine protein phosphatase calcineurin/PP2B, the DNA/RNA-directed alkaline phosphatase CIP, and three other metabolite-directed HAD phosphatases, namely NANP, NT5C1A and PNKP. PP2B, CIP and NANP were not inhibited by 7,8-DHF. Similar to PTP1B, PNKP activity was attenuated ( $\sim$ 30%) only at 40  $\mu$ M 7,8-DHF. In contrast, 7,8-DHF effectively inhibited NT5C1A (IC<sub>50</sub>  $\sim$ 10  $\mu$ M). NT5C1A is an AMP hydrolase expressed in skeletal muscle and heart. To our knowledge, a role of NT5C1A in the brain has not been reported. Based on currently available information, the inhibition of NT5C1A therefore appears unlikely to contribute to 7,8-DHF effects in the brain.

The results of these experiments are shown in the revised Figure 2d. Taken together, the extended selectivity analysis of 7,8-DHF on a total of 12 structurally and functionally diverse protein- and nonprotein-directed phosphatases supports our initial conclusion that 7,8-DHF preferentially inhibits PDXP.

*(2) Line 144: It is unclear how fig 2c supports the statement here. Remove call out for clarity.*

Our intention was to highlight the fact that 7,8-DHF concentrations  $>12.5 \mu\text{M}$  could not be tested in the BLI assay (shown in Figure 2c) due to 7,8-DHF solubility issues under these experimental conditions. However, since this is discussed in the text, but not directly visible in Figure 2c, we agree with the Reviewer and have removed this call out.

*(3) Figure 3a. It is difficult to see the pink 7,8 DHF on top of the pink ribbon backbone. A better combination of colours could be used. Likewise in Figure 3b it is pink on pink again.*

We have improved the combination of colors to enhance the visibility of 7,8-DHF and have consistently color-coded murine and the new human PDXP structures throughout the manuscript.

*(4) Figure 3c and d. These are the two protomers I believe, but the colour coding is not present in 3c where the ribbon is now gray. Please choose colours that can be used to encode protomers throughout the figure.*

Please see response to point 3 above.

*(5) Figure 3f. I think this is the same protomer as 3c but a 180-degree rotation. Could this be indicated, or somehow lined up between the two figures for clarity? It would also be useful to have 3e in the same orientation as 3f, to better visualise the overlap with PLP binding. PLP and 7,8 DHF could be labelled similarly to the amino acids in 3f (the colour coding here is helpful).*

Please see response to point 3 above. We have substantially revised the structural figures and have used consistent color coding and the same perspective of 7,8-DHF in the PDXP active sites.

*(6) Figure 3g. The colours of the bars relating to specific mutations do not quite match the colours in Figure 3f, which I think was the aim and is very helpful.*

We have adapted the colours of the residues in Figure 3f (now Fig. 3b and additionally Fig. 3 – figure supplement 1e) so that they exactly match the colours of the bars in Figure 3g (now Fig. 3d).

No further comments.

**Reviewer #3:**

*Page 4: The authors describe 7,8DHF as a "selective" inhibitor of PDXP - in my opinion, they do not have sufficient data to support such a strong assertion. Reports that 7,8DHF may act as a TRK-B-agonist already highlight a potential problem of off-target effects. Does 7,8DHF promote tyrosine phosphorylation of TRK-B in their hands? The selectivity panel presented in Figure 2, focusing on 5 other HAD phosphatases, is much too limited to support assertions of selectivity.*

We agree with the Reviewer that our previous selectivity analysis with six HAD phosphatases was limited. To further explore the phosphatase target spectrum of 7,8-DHF, we have now analyzed six other enzymes: three other non-HAD phosphatases (the tyrosine phosphatase PTP1B, the serine/threonine protein phosphatase PP2B/calcineurin, and the DNA/RNA-directed alkaline phosphatase/CIP) and three other non-protein-directed C1/C0-type HAD

**Reviewer #2:**

No further comments.

**Reviewer #3:**

*Page 4: The authors describe 7,8DHF as a "selective" inhibitor of PDXP - in my opinion, they do not have sufficient data to support such a strong assertion. Reports that 7,8DHF may act as a TRK-B-agonist already highlight a potential problem of off-target effects. Does 7,8DHF promote tyrosine phosphorylation of TRK-B in their hands? The selectivity panel presented in Figure 2, focusing on 5 other HAD phosphatases, is much too limited to support assertions of selectivity.*

We agree with the Reviewer that our previous selectivity analysis with six HAD phosphatases was limited. To further explore the phosphatase target spectrum of 7,8-DHF, we have now analyzed six other enzymes: three other non-HAD phosphatases (the tyrosine phosphatase PTP1B, the serine/threonine protein phosphatase PP2B/calcineurin, and the DNA/RNA-directed alkaline phosphatase/CIP) and three other non-protein-directed C1/C0-type HAD phosphatases (NT5C1A, NANP, and PNKP). The C1-capped enzymes NT5C1A and NANP were chosen because we previously found them to be sensitive to small molecule inhibitors of the PDXP-related phosphoglycolate phosphatase PGP (PMID: 36369173). PNKP was chosen to increase the coverage of C0-capped HAD phosphatases (previously, only the C0-capped MDP1 was tested).

We found that calcineurin, CIP and NANP were not inhibited by up to 40  $\mu$ M 7,8-DHF. The activities of PTP1B or PNKP activity were attenuated (by ~20 or 30%, respectively) only at 40  $\mu$ M 7,8-DHF. In contrast, 7,8-DHF effectively inhibited NT5C1A (IC<sub>50</sub> ~10  $\mu$ M). We have previously found that NT5C1A was sensitive to small-molecule inhibitors of the PDXP paralog PGP, although these molecules are structurally unrelated to 7,8-DHF (PMID: 36369173). NT5C1A is an AMP hydrolase expressed in skeletal muscle and heart (PMID: 12947102). To our knowledge, a role of NT5C1A in the brain has not been reported. Based on currently available information, the inhibition of NT5C1A therefore appears unlikely to contribute to 7,8-DHF effects in the brain. The results of these experiments are shown in the revised Figure 2d. Taken together, the extended selectivity analysis of 7,8-DHF on a total of 12 structurally and functionally diverse protein- and non-protein-directed phosphatases supports our initial conclusion that 7,8-DHF preferentially inhibits PDXP. To nevertheless avoid any overstatement, we have now also replaced "selective" by "preferential" in this context throughout the manuscript.

We have not tested if 7,8-DHF promotes tyrosine phosphorylation of TRK-B. Being able to detect 7,8-DHF-induced TRK-B phosphorylation in our hands would not exclude an additional role for PDXP/vitamin B6-dependent processes. Not being able to detect TRK-B phosphorylation may indicate absence of evidence or evidence of absence. This would neither conclusively rule out a biological role for 7,8-DHF-induced TRK-B phosphorylation in vivo, nor contribute further insights into a possible involvement of vitamin B6-dependent processes in 7,8-DHF induced effects.

*Page 6: The authors report that they obtained only two PDXP-selective inhibitor hits from their screen; 7,8DHF and something they describe as FMP-1. For the later, they state that it "was obtained from an academic donor, and its structure is undisclosed for intellectual property reasons". In my opinion, this is totally unacceptable. This is an academic research publication. If the authors wish to present data, they must do so in a manner that allows a reader to assess their significance; in the case of work with small molecules*

*that includes the chemical structure. In my opinion, the authors should either describe the compound fully or remove mention of it altogether.*

We are unable to describe “FMP-1” because its identity has not been disclosed to us. The academic donor of this molecule informed us that they were not able to permit release of any details of its structure or general structural class due to an emerging commercial interest.

We mentioned FMP-1 simply to highlight the fact that the screening campaign yielded more than one inhibitor. FMP-1 was also of interest due its complete inhibition of PDXP phosphatase activity.

Because the structure of this molecule is unknown to us, we have now removed any mention of this compound in the manuscript. For the same reason, we have removed the mention of the inhibitor hits “FMP-2” and “FMP-3” in Figure 2 – figure supplement 1 and Figure 2 – figure supplement 2. The number of PDXP inhibitor hits in the manuscript has been adapted accordingly.

*Page 7: The observed plateau at 50% inhibition requires further explanation. It is not clear how poor solubility of the compound explains this observation. For example, the authors state that “due to the aforementioned poor solubility of 7,8DHF, concentrations higher than 12.5µM could not be evaluated”. Yet on page 8, they describe assays against the specificity panel at concentrations of compound up to 40µM. Do the analogues of 7,8DHF (Fig 2b) result in >50% inhibition at higher concentrations? Further explanation and data on the solubility of the compounds would be of benefit.*

We currently do not have a satisfactory explanation for the apparent plateau of ~50% PDXP inhibition by 7,8-DHF. Resolving this question will likely require other approaches, including computational chemistry such as molecular dynamics simulations, and we feel that this is beyond the scope of the present manuscript.

We previously speculated that the limited solubility of 7,8-DHF may counteract a complete enzyme inhibition if higher concentrations of this molecule are required. Specifically, we referred to Todd et al. who have performed HPLC-UV-based solubility assays of 7,8-DHF (ref. 35). These authors found that immediately after 7,8-DHF solubilization, nominal 7,8-DHF concentrations of 5, 20 or 50 µM resulted in 0.5, 3.0 or 13 µM of 7,8-DHF in solution of (i.e., 10, 15 or 26% of the respective nominal concentration). Seven hours later, 46, 26 or 26% of the respective nominal 7,8-DHF concentrations were found in solution. Hence, above a nominal concentration of 5 µM, 7,8-DHF solubility does not increase linearly with the input concentration, but plateaus at ~20% of the nominal concentration. This phenomenon could potentially contribute to the apparent plateau of human or murine PDXP inhibition by 7,8-DHF in vitro.

However, experiments performed during the revision of our manuscript show that they HAD phosphatase NT5C1A can be effectively inhibited by 7,8-DHF with an IC50-value of 10 µM (see revised Fig. 2). Together with the fact that the activity of the PDXP-Asn61Ser variant can be completely inhibited by 7,8-DHF (see Fig. 3d), we conclude that the reason for the observed plateau of PDXP inhibition is likely to be primarily structural, with Asn61 impeding 7,8-DHF binding. We have therefore removed the mention of the limited solubility of 7,8-DHF here. On p.14, we now say: “These data also suggest that Asn61 contributes to the limited efficacy of 7,8-mediated PDXP inhibition in vitro.”

The solubility of 7,8-DHF is dependent on the specific assay and buffer conditions. In BLI experiments, interference patterns caused by binding of 7,8-DHF in solution to biotinylated PDXP immobilized on the biosensor surface are measured. In phosphatase selectivity assays, phosphatases are in solution, and the effect of 7,8-DHF on the phosphatase activity is measured via the quantification of free inorganic phosphate.

In BLI experiments, we observed that the sensorgrams obtained with the highest tested 7,8-DHF concentration (25  $\mu\text{M}$ ) showed the same curve shapes as the sensorgrams obtained with 12.5  $\mu\text{M}$  7,8-DHF. This contrasts with the expected steeper slope of the curves at 25  $\mu\text{M}$  vs. 12.5  $\mu\text{M}$  7,8-DHF. The same behavior was observed for the reference sensors (i.e., the SSA sensors that were not loaded with PDXP, but incubated with 7,8-DHF at all employed concentrations for referencing against nonspecific binding of 7,8-DHF to the sensors). The sensorgrams at 25  $\mu\text{M}$  7,8-DHF were therefore not included in the analysis (this is now specified in the Materials and Methods BLI section on p.27). To clarify this point, we now state that “As a result of the poor solubility of the molecule, a saturation of the binding site was not experimentally accessible” (p.7).

In contrast, the phosphatase selectivity assays described on p.8 could be performed with nominal 7,8-DHF concentrations of up to 40  $\mu\text{M}$ . Although the effective 7,8-DHF concentration in solution is expected to be lower (see ref. 35 and discussed above), the limited solubility of 7,8-DHF in phosphatase assays does not prevent the quantification of free inorganic phosphate. Nevertheless, we cannot exclude some interference with this absorbance-based assay (e.g., due to turbidity caused by insoluble compound). Indeed, 5,6-dihydroxyflavone and 5,6,7-trihydroxyflavone caused an apparent increase in PDXP activity at concentrations above 10  $\mu\text{M}$  (see Figure 2b), which may be related to compound solubility issues. Alternatively, these flavones may activate PDXP at higher concentrations.

We have tested the 7,8-DHF analogue 3,7,8,4'-tetrahydroxyflavone at concentrations of 70 and 100  $\mu\text{M}$ . At concentrations >100  $\mu\text{M}$ , the DMSO concentration required for solubilizing the flavone interferes with PDXP activity. PDXP inhibition by 3,7,8,4'-tetrahydroxyflavone was slightly increased at 70  $\mu\text{M}$  compared to 40  $\mu\text{M}$  (by ~18%) but plateaued between 70 and 100  $\mu\text{M}$ . These results are now mentioned in the text (p.7): “The efficacy of PDXP inhibition by 3,7,8,4'-tetrahydroxyflavone was not substantially increased at concentrations >40  $\mu\text{M}$  (relative PDXP activity at 40  $\mu\text{M}$ :  $0.46 \pm 0.05$ ; at 70  $\mu\text{M}$ :  $0.38 \pm 0.15$ ; at 100  $\mu\text{M}$ :  $0.37 \pm 0.09$ ; data are mean values  $\pm$  S.D. of n=6 experiments).”

*Page 9: The authors report that PDXP crystallizes as a homodimer in which 7,8DHF is bound only to one protomer. Is the second protomer active? Does that contribute to the 50% inhibition plateau? If Arg62 is mutated to break the salt bridge, does inhibition go beyond 50%?*

We have no way to measure the activity of the second, inhibitor-free protomer in murine PDXP. We know that PDXP functions as a constitutive homodimer, and based on our current understanding, both protomers are active. We have previously shown that the experimental monomerization of PDXP (upon introduction of two-point mutants in the dimerization interface) strongly reduces its phosphatase activity. Specifically, PDXP homodimerization is required for an inter-protomer interaction that mediates the proper positioning of the substrate specificity loop. Thus, homodimerization is necessary for effective substrate coordination and -dephosphorylation (PMID: 24338687).

In the murine structure, we observed that 7,8-DHF binding to the second subunit (the B-protomer) is prevented by a salt bridge between Arg62 and Asp14 of a symmetry-related A-protomer in the crystal lattice (i.e., this is not a salt bridge between Arg62 in the B-protomer and Asp14 in the A-protomer of a PDXP homodimer). As suggested, we have nevertheless tested the potential role of this salt bridge for the sensitivity of the PDXP homodimer to 7,8-DHF.

The mutation of Arg62 is not suitable to answer this question, because this residue is involved in the coordination of 7,8-DHF (see Figure 3b), and the PDXP-Arg62Ala mutant is inhibitor resistant (see Figure 3d). We have therefore mutated Asp14, which is not involved in 7,8-DHF coordination. As shown in the new Figure 3 – figure supplement 1d, the 7,8-DHF-mediated inhibition of PDXPAsp14Ala again reached a plateau at ~50%. This result suggests that while

an Arg62-Asp14 salt bridge is stabilized in the murine crystal, it is not a determinant of the active site accessibility of protomer B in solution.

To address this important question further, we have now also generated co-crystals of human PDXP bound to 7,8-DHF, and refined two structures to 1.5 Å. We found that in human PDXP, both protomers bind 7,8-DHF. These new, higher resolution data are now shown in the revised Figure 3 and its figure supplements, and we have moved the panels referring to the previously reported murine PDXP structure to the Figure 3 – figure supplement 1. Thus, both protomers of human PDXP, but only one protomer of murine PDXP bind 7,8-DHF in the crystal structure, yet the 7,8-DHF-mediated inhibition of human and murine PDXP plateaus at ~50% under the phosphatase assay conditions (see Figure 2a). We conclude that 7,8-DHF binding efficiency in the PDXP crystal does not necessarily reflect its inhibitory efficiency in solution.

Taken together, these data indicate that the apparent partial inhibition of murine and human PDXP phosphatase activity by 7,8-DHF in our in vitro assays is not explained by an exclusive binding of 7,8DHF to just one protomer of the homodimer.

*Page 10-12; Is it possible to generate a mutant form of PDXP in which activity is maintained but inhibition is attenuated - an inhibitor-resistant mutant form of PDXP? Can such a mutant be used to assess on-target vs off-target effects of 7,8DHF in cells?*

This is an excellent point, and we agree with the Reviewer that such an approach would provide further evidence for cellular on-target activity of 7,8-DHF. Indeed, the verification of the PDXP-7,8DHF interaction sites has led to the generation of catalytically active, inhibitor-resistant PDXP mutants, such as Tyr146Ala and Glu148Ala (Fig. 3d). However, the biochemical analysis of such mutants in primary hippocampal neurons is a very difficult task.

Primary hippocampal neurons are derived from pooled, isolated hippocampi of mouse embryos and are subsequently differentiated for 21 days in vitro. The resulting cellular yield is typically low and variable, and the viability (and contamination of the respective cultures with e.g. glial cells) varies from batch to batch. Although such cell preparations are suitable for electrophysiological or immunocytochemical experiments, they are far from ideal for biochemical studies. A meaningful experiment would require the efficient expression of a catalytically active, but inhibitor-resistant PDXP-mutant in PDXP-KO neurons. In parallel, PDXP-KO cells reconstituted with PDXP-WT (at phosphatase activity levels comparable with the PDXP mutant cells) would be needed for comparison. Unfortunately, the generation of (a) sufficient numbers of (b) viable cells that (c) efficiently express (d) functionally comparable levels of PDXP-WT or -mutant for downstream analysis (PLP/PL-levels upon inhibitor treatment) is currently not possible for us.

Human iPSC-derived (hippocampal) spheroids are at present no alternative, due to the necessity of generating PDXP-KO lines first, and the difficulties with transfecting/transducing them. Such a system would require extensive validation. We have attempted to use SH-SY5Y cells (a metastatic neuroblastoma cell line), but PDXK expression in these cells is modest and they produce too little PLP. We therefore feel that this question is beyond the scope of our current study.